2003

Hydrogenated microcrystalline silicon germanium material and photovoltaic devices prepared using ECR PECVD

Jianhua Zhu
Iowa State University

Hydrogenated microcrystalline silicon germanium material and photovoltaic devices prepared using ECR PECVD

by

Jianhua Zhu

A dissertation submitted to the graduate faculty

in partial fulfillment of the requirements for the degree of

DOCTOR OF PHILOSOPHY

Major: Electrical Engineering

Program of Study Committee:
Vikram Dalal, Major Professor
Alan Constant
Joeseph Shinar
Gary Tuttle
Robert Weber

Iowa State University

Ames, Iowa

2003

Graduate College
Iowa State University

This is to certify that the doctoral dissertation of

Jianhua Zhu

has met the dissertation requirements of Iowa State University

Signature was redacted for privacy.

Major Professor

Signature was redacted for privacy.

For the Major Program

TABLE OF CONTENTS

LIST OF FIGURES

LIST OF TABLES

ABSTRACT

High quality μc-SiGe:H is a very promising alternative for high efficiency photovoltaic device. The preparation of this material requires very high hydrogen dilution ratio in PECVD system. The deposition rate was greatly limited by this high hydrogen ratio. In this work, ECR PECVD technique is used to deposit μc-SiGe:H material. The growth rate can be greatly enhanced by taking advantage of the high plasma density and low ion energy features of ECR and extremely high hydrogen dilution ratios are no longer necessary for μc-SiGe:H growth. Films with good crystallinity were prepared at hydrogen dilution ratio as low as 1:15. An intensive study has been completed for the μc-SiGe:H with 0 to over 75% Ge incorporated. The optical bandgap shrinks with the incorporation of Ge into the material. Raman spectra and the increase of activation energy and photosensitivity indicates the deterioration of crystallinity by adding Ge to the Si structure. Solar cell devices using μc-SiGe:H as the active layer were deposited on stainless steel substrates. Fill factors over 55% were achieved for μc-SiGe devices with less than 35% Ge. An μc-Si buffer layer between n^+ and μc-SiGe:H n layer was used in the device design and this buffer layer revealed to be very beneficial to the device performance and the growth rate of μc-SiGe:H active layer. C-V measurements showed that the accidental oxygen leakage can raise the doping level to the order of 1E17cm^{-3}. ppm level TMB can be mixed in the source gas to very effectively reduce the N-type doping brought by oxygen. Short circuit current was increased by the TMB counter doping. The minority carrier diffusion length was estimated from reversed bias QE and C-V measurements. In the μc-SiGe:H devices fabricated by ECR PECVD, the hole

diffusion length is several tenth micrometers. The accidental doping in the μc-SiGe:H deteriorates the device performance by decreasing the minority carrier diffusion length. Compensating doping of TMB can increase minority carrier diffusion length L_p and improve short circuit current, and hence improve the conversion efficiency of solar cell device.

CHAPTER 1. INTRODUCTION

Hydrogenated Silicon based materials have attracted extensive attention of research in the recent years because of the applications in thin film photovoltaic devices. Among these applications amorphous silicon and amorphous silicon germanium solar cells have been brought to the threshold of large-scale commercialization. However, the amorphous active layer in solar cell devices suffers from the light induced degradation effects [1], which gradually deteriorates the performance of the solar cells. As a possible candidate to avoid this effect, microcrystalline silicon (μc-Si) has been considered as the next generation thin-film material for solar cell devices because it exhibit little light-induced degradation like amorphous silicon [2, 3] Stabilized efficiency of ~12% has already been obtained for a-Si/poly-Si tandem cell [4]. Unfortunately μc-Si requires a much thicker material (>2 μm) to absorb sufficient light due to the smaller light absorption coefficient. Very high growth rate are necessary to produce μc-Si solar cells for practical production. Some research groups have reported high rate deposition for small size μc-Si solar cells by using Very High Frequency Plasma Enhanced Chemical Vapor Deposition (VHF-PECVD), microwaves and so on. However it appears to be difficult to be applied on large substrate size and the product throughput can still not be improved.

Amorphous Silicon Germanium (a-SiGe) material has shown its advantages in enhancing the optical absorption of solar spectrum, especially in the near-infrared range for its lower bandgap compared to a-Si. The bandgap of a-SiGe can be tuned by adjusting the Ge concentration in the material. So it has been used as the absorption layer in the bottom of a

tandem solar cell to catch the infrared range photons. For its amorphous structure, it again suffers from the light degradation effects as a-Si does [5].

Either of the two problems, light-induced degradation for a-Si/SiGe or low optical absorption for μc-Si, exists until a proper combination of the advantages of these materials can be brought without the disadvantages. In this research project, hydrogenated microcrystalline silicon germanium (μc-SiGe:H) is intensively investigated as a solution. The microcrystalline structure of this material counter vent the light induced degration problem and ensures the reliability of solar cell application, while the incorporation of Ge into Si can considerably promote the absorption by lowering the bandgap of the material. Therefore, thin film photovoltaic device (typically in p-i-n or n-i-p structures) can absorb the sunlight efficiently with an active intrinsic layer less than 1um. Productivity can be improved and the cost expected to be reduced. Another advantage of μc-SiGe over μc-Si is that the material's optical and electrical properties can be precisely controlled by tuning the Ge content.

Unfortunately, it has been observed that the quality of μc-SiGe films seriously deteriorates with the incorporation of Ge. How to fabricate device-quality μc-SiGe films and apply to solar cells with good conversion efficiency is the min objective of this research.

1.1 Microcrystalline Si/SiGe Materials

There are four types of structures for Si based material: crystalline, polycrystalline, microcrystalline and amorphous. Among them crystalline silicon wafers and poly silicon films have been used in micro-circuit fabrication for decades. Microcryalline and amorphous silicon materials have found wide application in thin solar cells and thin film transistor arrays

for flat panel displays. The major difference between these structures is the dimension of the crystal in the material, as shown in the table below.

Table 1.1 Differences between various Si material structures and properties.

	Grain size	Structure	Applications
Crystalline Silicon (c-Si)	>100 um	Single crystallites same orientation	Micro-chip fabrication
Polycrystalline Silicon	1-100 um	Medium size crystallites at various orientations	Micro fabrication, TFT display
Microcrystalline Silicon (uc-Si)	<1 um	Small size crystallites at various orientations	TFT display, photovoltaic devices
Amorphous Silicon (a-Si)	<10 nm	Random orientation	TFT display, photovoltaic devices

1.1.1 Structure of microcrystalline Si/SiGe materials

Microcrystalline structure consists of nanometer sized crystal grains, grain boundaries and amorphous tissues. The crystallites often form columns growing perpendicular to the substrate surface. Around these columns are nanoscale disordered (amorphous) grain boundaries. A schematic of the microcrystalline structure is shown in Fig 1.1.

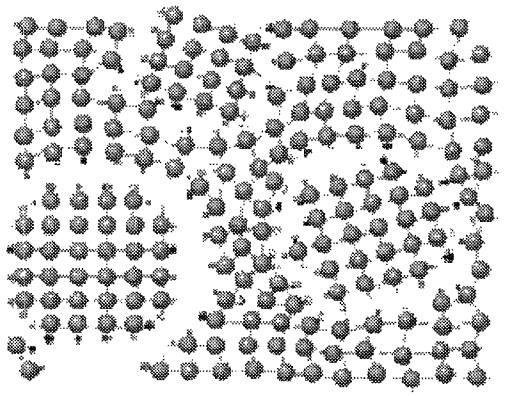

FIG. 1.1 Schematic drawing of microcrystalline material (provided by National Institute of advanced Industrial Science and Technology).

As a result, the carrier transport in microcrystalline silicon is affected by the carrier trapping and recombination via defects. Therefore, defects such as dangling bonds (DB) are efficiency-reducing objects with respect to solar cell applications. However, it appears that the structure of μc-Si/SiGe materials is largely independent of the method used for preparation.

1.1.2 Optical properties

The key feature of microcrystalline material is its dependence on the crystallinity of the structure. For μc-Si:H, at high photon energies (>2 eV), the absorption is lower than that of a-Si:H owing to there being a smaller volume fraction of amorphous tissue. It is suggested that at larger photon energies more carrier will be generated in the amorphous than in the crystalline phase [6]. In the low-energy range (<2 eV), the absorption increases with increasing crystallinity, indicating an increase in free-carrier absorption.

Raman spectroscopy has shown the different optical responses between microcrystalline and amorphous materials. The different optical responses root from the different microstruture. A typical Raman peak for μc-Si is at 520 cm-1 due to the Si-Si bond TO vibration. In μc-SiGe material, there are three bond configurations: Si-Si, Si-Ge and Ge-Ge, and three peaks at 520, 400 and 300 cm^{-1}. Actually the locations of these peaks in μc-SiGe material usually shift according to the Ge concentration in the material because the bond structure changes. For example, more Ge incorporation forms more Ge related bonds and reduces the Si-Si bonds, and the Si-Si peak will shift to the lower wave numbers due to the stress caused by the more Ge-Ge and Si-Ge bonds.

1.1.3 Electrical properties

The conductivity of microcrystalline material is also dependant on the crystallinity. Typical light conductivity values for μc-Si and μc-SiGe material are on the order of 10^{-6} to 10^{-5} S/cm under 1AM light intensity. However, the dark conductivity can range from 10^{-5} to 10^{-10} for different material structures such as the crystallinity, the doping level and the Ge concentration in μc-SiGe.

Due to the lower bandgap of the microcrystalline material, the conductivity activation energy E_A is lower in intrinsic μc-Si/SiGe materials than in a-Si/SiGe. As the bandgap, E_A is also dependant on the crystallinity level.

Hall mobility is much lower in microcrystalline materials due to the inhomogeneous struture than in the crystalline counterparts. For intrinsic μc-Si, a typical hole mobility value is on the order of 1 $cm^2/(sec\text{-}V)$, much lower compared to 400 $cm^2/(sec\text{-}V)$ in c-Si wafers. μc-SiGe carrier mobilities are comparable or even lower than μc-Si. The incorporation of Ge even randomize the structure and the more inhomogeneous structure hinders the transport of carriers.

Unlike the carrier transport in amorphous material, the carrier transport in microcrystalline material is anisotropic. The conductivities parallel and perpendicular to the substrate differ due to the columnar feature of the crystallites.

1.2 μc-Si/SiGe p-i-n Solar Cell Devices

There are two types of thin film solar cells structures: p-i-n structure and n-i-p structure [7], depend on the different growth orders and the type of the substrate. Solar cells in p-i-n structure have shown better conversion efficiency for various reasons such as better interface

properties and less Boron diffusion problems. A typical p-i-n solar cell structure is shown in Fig 1.2.

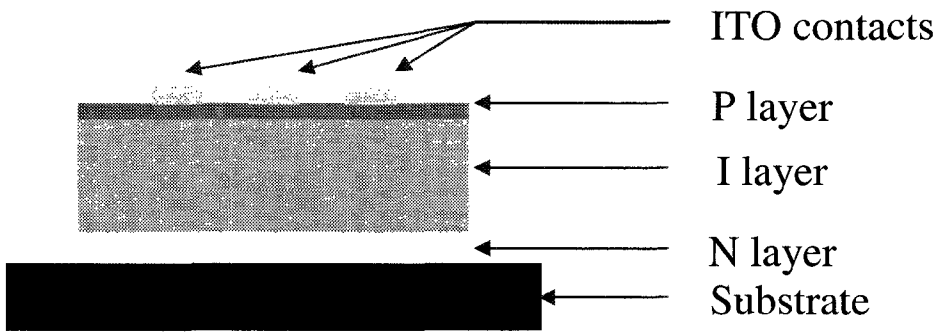

FIG 1.2 A schematic of a typical p-i-n solar cell device

A stainless steel substrate is usually cleaned before loading for film growth. Usually a conducting textured layer such as ZnO is deposited on the substrate to enhance the photon absorption and increase the conversion efficiency. A p-doped n^+ amorphous or microcrystalline Si layer about 100 nm thick is deposited on the substrate. Then the intrinsic microcrystalline layer is grown on the top of n^+ layer and the typical thickness of this layer varies for μc-Si and μc-SiGe cells. A μc-Si cell needs up to 2 um thick for this main absorption layer, while μc-SiGe cell only needs about 0.5 um. The fact that an amorphous incubation layer of about 100 A thick is often grown before the microcrystalline structure forms, especially on foreign substrate such as glass or amorphous layer. A high quality active microcrystalline active layer is a must for a high conversion efficiency device. Recombination rate in this layer should be minimized for the best collection of photo-generated carriers. Following the intrinsic layer is the Boron doped p+ layer in the cell. Microcrystalline layer is used for better conductivity. This is the layer where the light enters

the cell. Since the absorption happening here needs to be minimized because the worse carrier transport in the doped structure, the thickness of the p^+ layer is limited to about 50 A. To let more photons come to the intrinsic active layer, a thin Si-C transition is often used as the window. Also the Si-C layers can be utilized to optimize the interface properties between p+ and I layer by reducing the Boron diffusion during the deposition process. Contacts of Al or ITO are evaporated or deposited on the surface using masks.

In microcrystalline solar cell devices, the minority carrier diffusion length is a key parameter to characterize the carrier transport, unlike in amorphous devices where the internal electric field dominates the carrier transport.

Due to the fact that oxygen is usually accidentally incorporated in the film growth in the CVD system, the intended intrinsic microcrystalline layer tends to be O-doped and hence becomes slightly n-type. Therefore the minority carrier in the active layer is holes. How to increase the hole diffusion length in the solar cell is a good topic to increase the conversion efficiency of microcrystalline solar cells.

1.3 Literature Review

A lot of work has been done on μc-Si thin films and solar cell devices, including the material preparation and characterization, solar cell physics modeling and etc. So far various deposition techniques have been investigated for μc-Si growth, such as PECVD [8-13], VHF PECVD [14, 15], ECR PECVD [16] and HW CVD [17, 18]. In most of the deposition processes, substrate [19], deposition temperature [20, 21] and H_2 dilution rate [21, 22, and 23] are recognized as the key parameters. The substrate selectivity can be explained on the basis of a-Si:H nucleation versus homogeneous growth mechanisms. It is expected that μc-Si

formation is favored on the substrates in which deposition proceeds via a nucleation (porous) phase [19]. The formation of μc-Si:H will first be enhanced by increasing temperature and then suppressed above 400 °C due to the escape of hydrogen atoms from the growing surface [24]. It is also found that the H_2 dilution rate is also one of the most common parameter to control the structure of the material and the crystalline volume fraction decreases with increasing SiH_4 and GeH_4 flow rates. Very high hydrogen dilution rate facilitates the microcrystallization and also reduces the deposition rate drastically. However, nears the transition to the amorphous growth regime the highest solar cell efficiency was achieved [25]. Real time spectroscope ellipsometry (SE) results revealed the μc-Si nucleation from hydrogenated amorphous silicon phase, followed by the coalescence of isolated μc-Si:H grains exposed in growing surfaces. The μc-Si:H nuclei density increases significantly as the hydrogen dilution ration increases[26]. The role of hydrogen in the crystallization process is extensively studied and there four growth proposals as to how atomic hydrogen promotes the formation of μc-Si.

Model 1 by Veprek et al. [27] proposed threat there is a partial chemical equilibrium during deposition between the μc-Si and a-Si:H. This led to the ides that μc-Si and a-Si:H are deposited simultaneously from the plasma, but the a-Si:H was selectively etched back to the plasma by atomic hydrogen.

Model 2 by Matsuda and Tanaka [28], Matsuda [29], Saitoh [30] et al., and Kondo et al. [31] is the surface mobility model, which has been applied to a-Si:H, its alloys and μc-Si. It was argued that hydrogen dilution provided a higher-surface coverage by Si-H groups. Thereby increasing the surface diffusion length of the SiH_3 growth species. This would allow

SiH_3 to find more stable growth sites to give better a-Si:H, and then to find the most stable growth site to form μc-Si.

A third model is the chemical annealing model of Nakata et al. [32], Shirai et al. [33], Nakamura [34] and Sriraman et al. [35]. It is observed that there can be subsurface crystallization of a-Si:H into μc-Si [35, 36, and 37]. It was proposed that hydrogen inserts into the a-Si:H atomic network, lowering the average coordination number, so that it becomes sufficiently flexible or floppy for the crystallization to occur.

The fourth model is Robertson's thermodynamic model of nucleation [38]. It claims that increasing the hydrogen content of the a-SiH_x precursor phase increases the relative stability of μc-Si slightly, but strongly increases the driving force for nucleation. The higher stability of μc-Si is the fundamental origin of the higher etch rates of a-Si:H. while surface mobility models do not account for subsurface nucleation of μc-Si.

Dalal's group produced high quality μc-Si thin films and solar cell devices with a low dilution ration of 8:1. It was found that once the crystallization started, one could decrease the hydrogen/silane ration and still obtain microcrystalline growth [16] Ion bombardment effects were studied and it suggested that the ion bombardment, and particularly the implantation of hydrogen ions, favors the formation of a porous layer where the nucleation of crystallite takes places [39].

As to the μc-SiGe material, there have not been reported study until 1996 when Ganguly et al [40] reported the μc-SiGe:H thin films prepared at very low growth rate (0.08A/s to 0.36A/s) using very high H2 dilution by rf PECVD method.. Optical absorption properties were investigated and it showed that the absorption in the long wavelength region was greatly enhanced by over 10 times. Two years later Ganguly et al studied the growth

chemistry of μc-SiGe comparing to μc-Si, and found the optimum hydrogen dilution (for a maximum grain size) decreases with growth temperature and the crystallization on-set hydrogen dilution was lower for μc-Si. In year 2000, both Dalal's group [41] and Isomura et al prepared solar cell devices using μc-SiGe as the active layer. Dalal's group used low pressure ECR deposition and Isomura used rf PECVD. These devices are with Ge concentrations less than 30%. The enhancement of QE in the low energy range was obtained. Huang and his colleagues investigated the transport properties of μc-SiGe films prepared by extremely high hydrogen dilution ratio (up to 500). [42] They found that crystallinity and grain size exerted a big influence on the transport mechanism, especially with very high hydrogen dilution (R>300), both of conductivity and mobility came to decrease and the electronic transport properties degrades. Rath, Tichelaar and Schropp prepared μc-SiGe solar cell device by rf PECVD at a substrate temperature of 195 °C [43]. A current density of 9.44 mA/cm2 was generated in an I-layer of only 150 nm thick without any back reflector. But no FF and QE data was reported.

1.4 Scale of Research

All the previous reports on μc-SiGe are incomplete. A full coverage of the Ge% is in need to investigate the material and device properties. Materials grown at different conditions are necessary to understand the transport properties. ECR PECVD method, proved to be beneficial for high quality amorphous/microcrystalline material growth due to the high density and low energy plasma, is expected to maintain the advantage when used to grow μc-SiGe at high growth rate.

There are two main objectives of this research project. First is to explore the optimum growth conditions using ECR PECVD for high quality μc-SiGe:H material with varying Ge concentration. By doing this we can study the growth chemistry and transport mechanism by incorporating different amount of Ge. Second is to make actual solar cell devices using μc-SiGe active layer of different Ge%. Since the bandgap of uc-SiGe can be tuned precisely by controlling the Ge concentration, μc-SiGe solar cell can be used in tandem cells for high conversion efficiency. In this project μc-SiGe solar cell devices grown at different conditions are also used to investigate the transport properties of microcrystalline materials.

For all the samples, thin films and n-i-p devices, electrical, optical and structural measurements, including conductivities, activation energy, optical absorption, crystallinity, composition, I-V characteristics and Quantum Efficiency etc, were studied.

CHAPTER 2. ECR PECVD GROWTH OF μc-SIGE

2.1 ECR System Overview

Electron Cyclotron Resonance technique has been widely used in research lab and industry as the plasma source of plasma deposition or high-density plasma etching. There are several technical advantages of ECR Plasma deposition compared to conventional glow discharge deposition. These advantages are: (1) high plasma density caused by the high ionization ratio; (2) low ion energy which avoids high-energy ion bombardment damaging to the growing surface; (3) lower operating pressure, which may lead to cleaner processing; (4) lower substrate temperature. The ECR plasma deposition also enables easy control of the dissociation of source gases and reduces powered electrode effects such as contamination, self-biasing and hot electron generation.

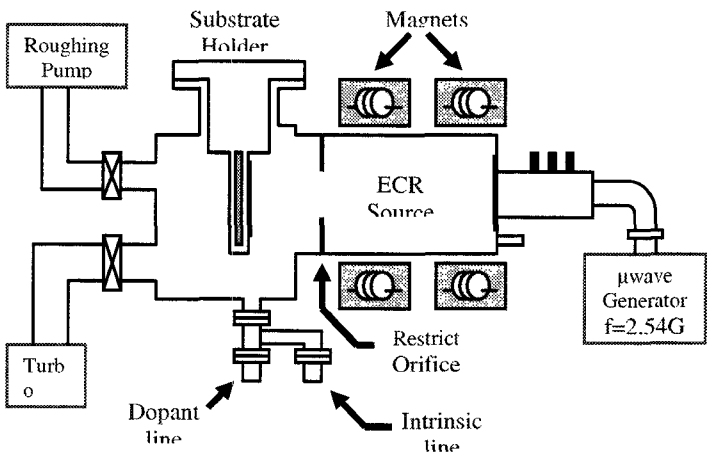

FIG. 2.1 ECR PECVD system schematic

A schematic of the ECR PECVD system used in this research project is shown in fig. 2.1. In this system the plasma source gas is introduced in to the excitation chamber while the

deposition source gases to the deposition chamber. Two coils surrounding the plasma excitation chamber generate a magnetic field in the amount of about 880 Gauss in the center of the chamber. Substrate temperature can be controlled by the electrical heater attached to the substrate holder. The basic principle is that the excitation chamber operates as a resonance cavity. The Lorentz Force by the magnetic field forces the electrons moving in a circular cyclotron track. And the highest plasma production efficiency is achieved when the frequency of electrons in circular motion reaches the microwave frequency. In this system, a 2.45 GHz microwave was used. The plasma is generated by electron transferring energy to plasma gas molecules and dissociating them into charged or neutral particles. These include ionized and excited molecules, neutral molecules and neutral and ionized fragments of broken-up molecules, including free radicals. Free radicals are electrically neutral species that have incomplete bonding, that is, they have unpaired electrons. These species are extremely reactive, and wit other species are absorbed onto the surface, migrate, interact, rearrange, and chemically recombine to form the film. In addition, ion and electron bombardment from the plasma onto the growth surface can occur. The plasma was extended into the deposition chamber by the divergent magnetic field and further dissociates the source gases in front of the substrate and grow on the substrate. The ECR plasma, because of the high frequency involved, produces ions of only about 10-15 eV energy [44], considerably less than the energy of ions in a RF glow discharge reactor, which may approach 50-100 eV under conditions typically used for microcrystalline growth. Also due to the very high-energy transfer efficiency between the electrons and the plasma source gas molecules, a very low pressure as low as 1 mTorr can still maintain stable plasma. The advantage of low pressure is that there is little reaction in the gas phase between the different radicals generated by the

plasma and then the higher order radicals such as Si_2H_5 do not play a role in the growth which makes the film more homogeneous. Indeed previous work in our group has shown that only small radicals such as SiHx, GeHx (x =1,2,3) play a role in the ECR growth [45]. More than 70% of the microwave power can be absorbed in the plasma. The microwave power required for stable plasma is reduced by one order of magnitude with respect to non-magnetically confined plasma.

2.2 Thin Film Deposition using ECR PECVD

μc-SiGe thin films are deposited on Corning 7059 glass substrates. The deposition pressure was chosen to be 5 mTorr and microwave power at 200 W. The reason for the relatively low pressure is that a higher H^*/H_2 ratio at the substrate is needed to prevent amorphous growth as opposed to microcrystalline growth. SiH_4, GeH_4 and H_2 are used as the source and plasma gases for the film growth. Different combinations of the flow rates of these gases are studied in the experiment. And also different substrate temperatures of 300 – 450 °C are investigated. Two parallel Cr contact bars are thermally evaporated onto the sample surface for conductivity measurement. Notice that this conductivity measured is only the parallel conductivity, but not the vertical conductivity which is the case in actual device operation.

There have been a lot of discussions on the topic of plasma deposition growth chemistry. [46-49]. It is generally believed that the deposition process can be described in four steps: (1) feed-stock source gases are dissociated in the region in front of the substrate; (2) dissociated species are adsorbed on the growing surface and attached; (3) strongly bonded species remain on the surface and forms the layer while weakly bonded species are etched out of the

surface by the plasma. (4) transport of byproducts out of the deposition region. The deposition rate can be limited by any of these steps, and like in ordinary CVD technique, the growth rate can be recognized as mass transfer controlled or surface reaction controlled. In the ECR PECVD system, there are several reactions happening near the substrate surface:

$$e + SiH_4 \leftrightarrow SiH_3 + H^+$$
$$e + SiH_3 \leftrightarrow SiH_2 + H^+$$
$$e + SiH_2 \leftrightarrow SiH + H^+$$
$$H^+ + SiH_4 \leftrightarrow SiH_3 + H_2$$
$$e + GeH_4 \leftrightarrow GeH_3 + H^+$$
$$e + GeH_3 \leftrightarrow GeH_2 + H^+$$
$$e + GeH_2 \leftrightarrow GeH + H^+$$
$$H^+ + GeH_4 \leftrightarrow GeH_3 + H_2$$

Since they are several different radicals formed in the plasma, the growth subsurface will be rough and forms many voids and dangling bonds [50]. One may expect to control the dominant growth radical to obtain homogeneous film growth. It is generally believed that SiH_3 and GeH_3 are dominant and the most important radicals for the growth.

Growth models

Basically, the growth models of microcrystalline material including μc-Si and μc-SiGe can be summarized into the two following types:

i. "surface"models in which μc-Si results from the details of the interaction of the plasma species with the growing surface. In these models the chemical equilibrium between the deposition and hydrogen etching [51] the selective etching of the amorphous phase of hydrogen atoms [52, 53] and the surface mobility of the film precursors [54] are considered.

ii. "growth zone" models in which the atomic hydrogen interact with the amorphous phase within a zone extending a few nm below the growth surface and thus produces its relaxation or chemical annealing [55, 56]

In the μc-SiGe deposition using ECR PECVD, the growth chemistry is even more complicated than in μc-Si growth. The incorporation of Ge radicals in the plasma makes the growth chemistry much more complicated. Because of the lower dissociation energy of Ge-H bond, GeH_4 is much more easier to break than SiH_4. This is why the actual Ge concentration in the material is usually higher than the GeH_4 percentage in the feed-stock gas. Another issue is that Ge atom is much heavier than Si atom, and hence the surface diffusion mobility is much lower. Ge atoms are more difficult to find the balanced site to bond and from a homogeneous network. A lot of defect states come from the voids and Ge-caused dangling bonds. How to control the growth process with Ge-incorporated plasma still remains a challenge to PECVD researchers.

2.3 Device Fabrication

All devices are in the conventional n-i-p configuration. As usual a stainless steel substrate of 1.5 inches by 1.5 inches is used for device growth. To simplify the process no textured structures were applied on the substrate. The substrate is cleaned using Acetone boiling and Methanol ultrasonic before loaded into the growth chamber. Up to 10 times N_2 purges are necessary to remove the residual gases in the chamber. The base pressure is on the order of 10^{-7} Torr for deposition. ppm level TMB is used to compensate the possible O_2 doping during the growth process.

In the μc-SiGe device configuration, they are some certain modifications compared to the μc-Si device. First of all, the main active layer tends to be accidentally doped although they are supposed intrinsic. Investigation has revealed that this is because of the very tiny amount of O leakage from outside the chamber. Therefore, the actual active layer of the cell is slightly n doped. From now on we call our device structure n^+-n-p^+. Secondly, the doped n^+ and p^+ layers are in amorphous Si, not a-SiGe or μc-SiGe. This is because we want to counter vent the doping complexity brought by the incorporation of Ge. Also a wider bandgap material is needed in the p^+ layer to allow more sunlight coming into the main absorbing layer of the cell. Since a-Si is used as the n^+ and p^+ layers, buffer layers are necessary to gradually transit from n^+ to n and from n to p^+. Very thin μc-Si layer in the order of 50-100 nm is used for the n^+-n transition, and n to p^+ transition was achieved by lowering GeH_4 flow rate gradually. So the real device structure of the μc-SiGe solar cell becomes as in fig 2.2.

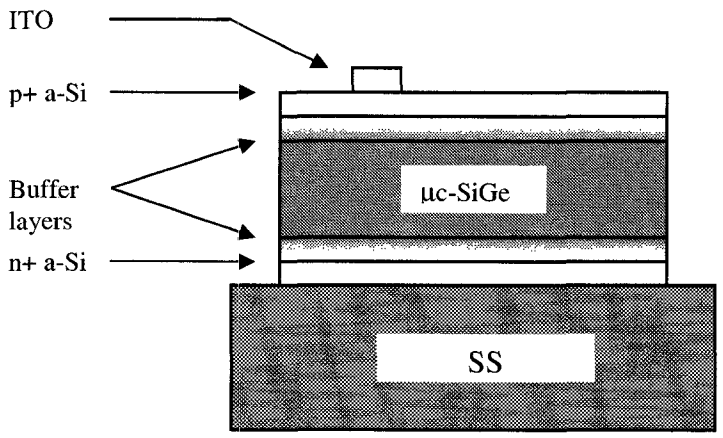

FIG. 2.2 The device structure of μc-SiGe:H solar cells

To allow photons coming into the cell, three semi-transparent ITO contact dots of about 0.077 cm^2 were deposited on the top of p^+ layer using a DC sputtering system. The

deposition temperature was 200C and pressure at 5 mTorr. In this process, an ITO target was sputtered by Ar+ ions and the atoms sputtered out from the target fall onto the device surface. About 1% O_2 was mixed in the Ar gas to compensate the possible loss of oxygen in the sputtering process. The thickness of the ITO contact used in this experiment was about 2500A.

2.4 Device Physics

As mentioned in the previous section, the solar cell devices are in n+-n-p+ structure. Buffer layers between n+ and n, n and p+ were used during the fabrication process to achieve higher device performance. A bandgap diagram of the device structure is shown in fig. 2.3.

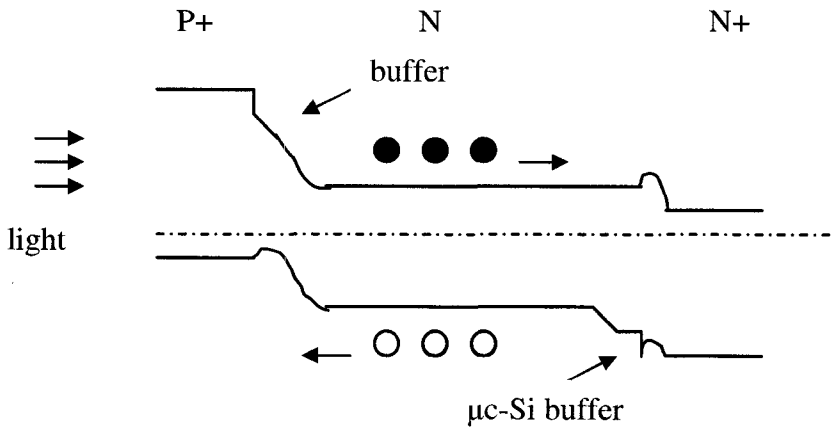

Fig. 2.3 The band diagram of μc-SiGe solar cell device.

As shown in the band diagram, the buffer layer in the p-n interface was used to grade the bandgap from small bandgap main active μc-SiGe layer to the wider bandgap amorphous SiC layer in the front end. The wide bandgap a-SiC material is necessary to let more light absorbed in the main μc-SiGe layer because the minority carriers generated in doped layers

usually recombine before being collected. Because of the bandgap discontinuity between a-SiC and μc-SiGe, holes are very easy to get trapped in the valence band notch if there is no buffer at the interface. The build in electric field produced by the band bending at this interface can drive the electrons away from the p layer and greatly enhance the collection efficiency.

We also used thin μc-Si buffer layer at the back interface(n+-n). There are two purposes of this buffer layer: 1) the incubation a-Si layer grown right on top of the N+ layer can seal up the possible shorts on the substrate and increase the shunt resistance of the cell; 2) the μc-Si layer can provide a built-in electric field and helps drive the holes to the p+ layer.

Both of these buffer layers have been shown very useful to improve carrier transport through the device and hence the solar conversion efficiency.

CHAPER 3. SAMPLE CHARACTERIZATIONS

Samples are routinely measured in a timely manner to study the optical, electrical and structural properties.

3.1 Optical Characterization

Optical characterizations include thickness measurement, optical absorption, infrared optical reflectance and conductivities. A comprehensive review of optical characterization methods for semiconductor materials can be found in the literature [57].

- Thickness

Reflectance curves were obtained using a UV/VIS/NIR lamda-9 spectrometer. For thickness measurement, the wavelength range was chosen to be 1000-2500 nm where the absorption is small enough and very strong reflective constructive and destructive peaks and valleys can be determined on the curve. Two adjacent peaks or valleys were located by the wavelengths and the thickness of the film was determined using the following equation:

$$t = \frac{\lambda_1 \times \lambda_2}{2n(\lambda_1 - \lambda_2)}$$

where $\lambda 1$ and $\lambda 2$ are the corresponding wavelengths of the adjacent peaks (valleys) chosen for thickness calculations; n is the index of refraction of the sample. For $\mu c\text{-}Si_{1-x}Ge_x$, the index of refraction can vary by different Ge concentration (different x) and at different wavelength range. In this experiment, we choose the peaks near by about 1200 nm range for more precise thickness calculation. The n values of different x can be acquired y obtaining the reflection spectra and solving for n:

$$Avg(R) = \frac{(n_1 - n_0)^2}{(n_1 + n_0)^2}$$

where Avg (R) is the average reflection in the long wavelength region.

- Optical absorption

The absorption spectra were obtained by combining the lamda-9 absorption data and the dual-beam photo-conductivity method developed by Wronski and co-workers [58]. An overlap of these two methods at 1000nm – 1100 nm was used to calibrate the two methods and normalize the absorption curve. For high energy photons (wavelength range of 500 nm – 1100 nm) the spectrometer data can give precise absorption coefficients because the absorption is strong. For longer wavelength range, the absorption is not so visible in the spectrometer data because of the strong reflective interferences. And the absorption data was this range was measured by the dual beam photo-conductivity method. This method can accurately measure the absorption below $10^2 cm^{-1}$. It utilizes a DC light beam to fix the quasi Fermi levels and hence maintain a constant carrier lifetime. The DC light continuously creates electron-hole pairs to keep traps filled and the occupancy of mid-gap states constant. And an ac light (at 13Hz) of low intensity was superimposed on the DC light on the sample surface and creates more electron-hole pairs. The frequency of the ac light was generated by an electrically controlled chopper in front of the lenses and it should not be multipliers or dividends of the room light frequency (50Hz) to avoid light interference. Lock-in amplifier was used to probe the changing photoconductivity caused only by the ac light. The absorption in the sample was calculated at each wavelength by dividing the signal by a reference signal and multiplying by the quantum efficiency of the Si and Ge reference detector. The absorption coefficient can be further calculated from the known thickness of

the sample. A schematic of the dual beam photoconductivity measurement instrument used in this experiment was shown in fig 3.1. A quartz lamp was used as the light source of the ac light and a monochrometer was used for different photon wavelength. The range was chosen to be 900 nm to 1600 nm for μc-SiGe films. The chopped light produced the ac light at 13 Hz. Two lenses and a highly reflective mirror were used to focus the light onto the small area between two contact bars on the sample. Three high pass filters at 700, 900 and 1220nm were used in the experiment to avoid second harmonics from the monochrometor and maintain the light intensity at a low level.

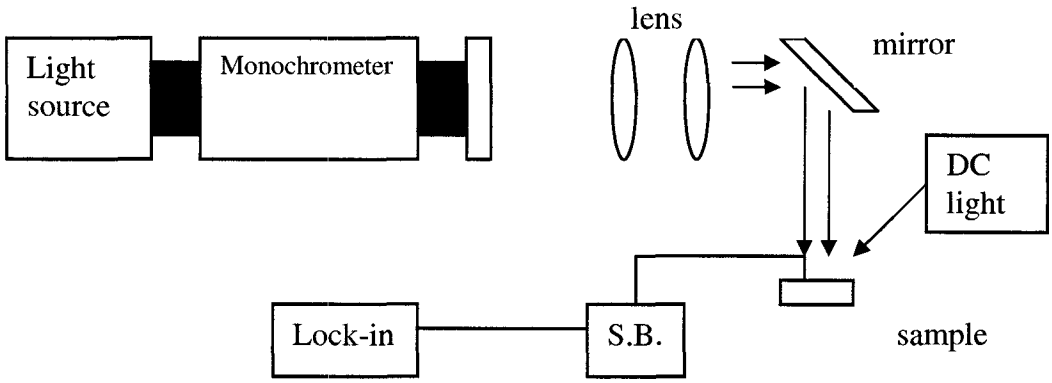

FIG. 3.1 Dual beam photoconductivity measurement instrument

The absorption curve was plotted against photon energy in a log scale. Like in amorphous materials, the photon energy where the absorption coefficient α is $10^4 cm^{-1}$ is called E_{04}. Amorphous silicon has a E_{04} value about 2 eV and microcrystalline silicon about 1.9 eV.

- Conductivity

Conductivities of the films were measured by applying 100 V between the two Cr electrodes and measuring the current at room temperature (25 °C). Since we know the dimension of the electrodes and the distance between, the conductivity can be calculated by:

$$\sigma = \frac{L}{W} \times \frac{I}{V \times t}$$

L is the length of the electrode and W is the distance between the electrodes; t is the thickness of the film; I and V are the current and applied voltage respectively. The current can be written in the form of carrier densities as following:

$$I = qnv = qE(\mu_n n + \mu_p p)$$

where E is the planar electric field between the electrodes; μ_n and μ_p are the drift mobility of electrons and holes respectively; n and p are the carrier density of electrons and holes in the material. Photoconductivity can be expressed in the following format:

$$\sigma_L = \Delta n q \mu = \alpha(1-R)\eta\tau\phi_{in}$$

where Δn is the excess carrier density generated by photons; α is absorption coefficient and η the quantum efficiency; τ is the lifetime of electrons and Φ_{in} is the incident photon intensity. Since α is always varying with the photon energy, precise determination is taken using filtered photons. Also high-energy photons are preferred to obtain the σ_D of the bulk instead of the sample surface.

We can see the photoconductivity is directly proportional to the current generated by the light shining. Different conductivity values can be produced by different amount of light intensity on the same material. In our experiment, the photoconductivity σ_L was measured under 1.5 Air-mass (AMS) lamp. A high photoconductivity is usually an indication of good quality material with low-level defect states. Dark conductivity is related to the intrinsic carrier density in the material. In σ_D measurement, all carriers are thermally excited if the film is intrinsic. The ratio of σ_L over dark conductivity σ_D is called photosensitivity. Intrinsic amorphous Si or SiGe material has a high photosensitivity up to 10^5 because of the relatively

high bandgap of the material compared to microcrystalline counterparts. In μc-Si/SiGe material, the optical bandgap is shifted to the lower photon energy, and there are much more intrinsic carriers than in amorphous materials (remember there is an exponential relation between the carrier density and the negative of bandgap). So for good microcrystalline Si or SiGe material, the photosensitivity can be as low as 1 because the material itself has a large amount of carriers comparable to or even higher than the photo-generated carrier density.

An measurement of the dark conductivity at different temperatures gives the activation energy (E_A). E_A is a measure of the difference between Fermi level to the conduction band edge. In this experiment, the dark conductivity was measured from 200 °C to 100 °C with 10 °C step. Arrhenius plots of σ_D show activated behavior

$$\sigma = \sigma_0 \exp\left(-\frac{E_A}{kT}\right)$$

E_A is about 0.8 eV for a-Si film, and a lower E_A value is expected for microcrystalline material because of the low bandgap. Accidental oxygen doping can also decrease E_A by moving the Fermi level upwards.

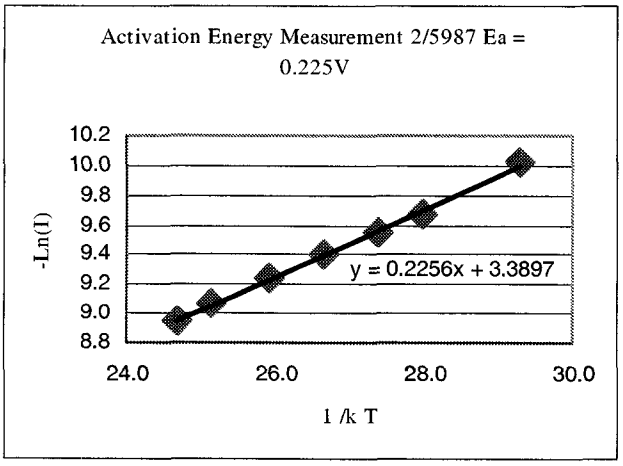

FIG. 3.2 Activation energy (E_A) measurement by measuring temperature effect on dark conductivity of thin film samples.

3.2 Structural Characterization

Structural characterizations were performed to study the crystallinity and composition of the samples. Raman spectroscopy and X-ray Diffraction were used to determine the crystallinity and grain size of both the film and devices. Energy Disperse Spectroscopy was used to get the compositional information in the samples.

- X-ray Diffraction

X-ray Diffraction was measured using a SIEMENS D500 x-ray diffractometer that is equipped with a diffracted beam monochrometor and a sample spinner. Cu Kα line (λ=1.542A) with step size of 0.05° of 2θ was used for this experiment. Microcrystalline silicon will show prominent peaks from the (111), (220) and (311) planes at about 28.1°, 47.2° and 55.5° respectively. With incorporation of Ge into the material, these peaks almost remain at the same locations. The average grain size in the material can be estimated using Scherrer's formular:

$$x = 0.94 \frac{\lambda}{B_{2\theta} \cos\theta_B}$$

where $B_{2\theta}$ is the full width in radians at half maximum intensity, if film is thick enough compared to the wavelength of the x-ray photons used.

- Raman Spectroscopy

Raman spectroscopy is the measurement of the wavelength and intensity of inelastically scattered light from molecules. The Raman effect arises when the incident light excites molecules in the sample which subsequently scatter the light. While most of this scattered

light is at the same wavelength as the incident light, some is scattered at a different wavelength. This inelastically scattered light is called Raman scatter. It results from the molecule changing its molecular motions.

The energy difference between the incident light (Ei) and the Raman scattered light (Es) is equal to the energy involved in changing the molecule's vibrational state (i.e. getting the molecule to vibrate, Ev). This energy difference is called the Raman shift.

$$Ev = Ei - Es$$

Several different Raman shifted signals will often be observed, each being associated with different vibrational or rotational motions of molecules in the sample. The particular molecule and it's environment will determine what Raman signals will be observed. A plot of Raman intensity vs. Raman shift is a Raman spectrum. For μc-Si, the Raman peak is at 520 cm^{-1} associated with the transverse optical (TO) mode of crystal silicon, whereas signals of a-Si appear around 480 cm^{-1}. In actual μc-Si film we can see both the 520 cm^{-1} sharp peak and the 480 cm^{-1} amorphous bump due to the existence of amorphous grain boundaries. For μc-SiGe material, there are three Raman peaks associated with three different bonding conditions: the Si-Si peak at around 510 cm^{-1}, the Si-Ge peak around 400 cm^{-1} and the Ge-Ge peak around 300 cm^{-1}. The actual locations of these peaks can shift with different Ge concentration due to the stress produced by Ge atoms in the material.

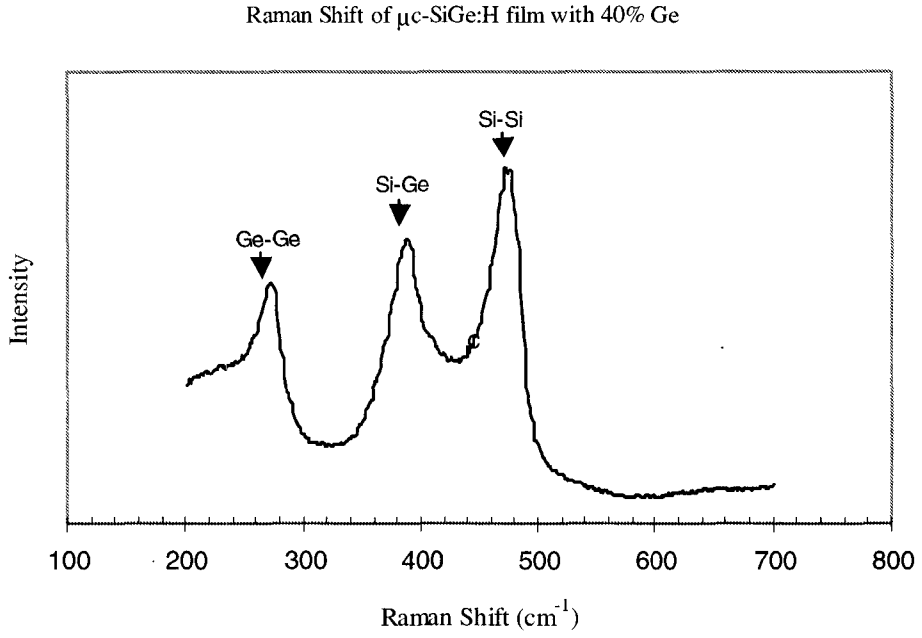

FIG. 3.3 Raman shift of μc-SiGe:H thin film with 40% Ge

In this experiment a Micro Raman Spectrometer with an Ar+ laser source was used. It is possible to compare the different area on the sample by focusing the laser light on different sites.

- Energy Dispersive X-ray Spectroscopy

EDS is also sometimes referred to as EDXA (energy dispersive x-ray analysis) or EDAX (energy dispersive analysis of x-rays). EDS operates by using a crystal of silicon or germanium to detect the x-rays. Each photon generates multiple electron-hole pairs equal in total energy to the energy of the photon (each pair has a fixed energy determined by the crystal). A voltage is applied to the crystal to separate the electrons and holes so that the charges appear as a small step-change in voltage. Pre-amplifiers and amplifiers process the

signal and pass it to a multi-channel analyzer (analog-to-digital converter) so that the x-ray spectrum can eventually be displayed as a histogram of x-ray intensity as a function of energy.

The EDS samples are thin films of ~1um deposited on stainless steel substrate.

3.3 Electrical Characterization

Electrical characterizations include I-V, C-V and quantum efficiency measurements for devices. The minority diffusion length can be estimated by combining the QE and C-V measurements.

- I-V characteristics

I-V behavior is one of the most important measurements for solar cells. It directly tells how good the device is and gives some information about where the problems are, if there are some. Our experiment used an ELH quartz lamp operating at 115 V, 2.4 Amp as the light source for I-V measurement. A typical I-V curve of a solar cell is shown in fig 3.4. In this figure, V_{oc} is the open circuit voltage, I_{sc} is the short circuit current of the cell and FF is the fill factor.

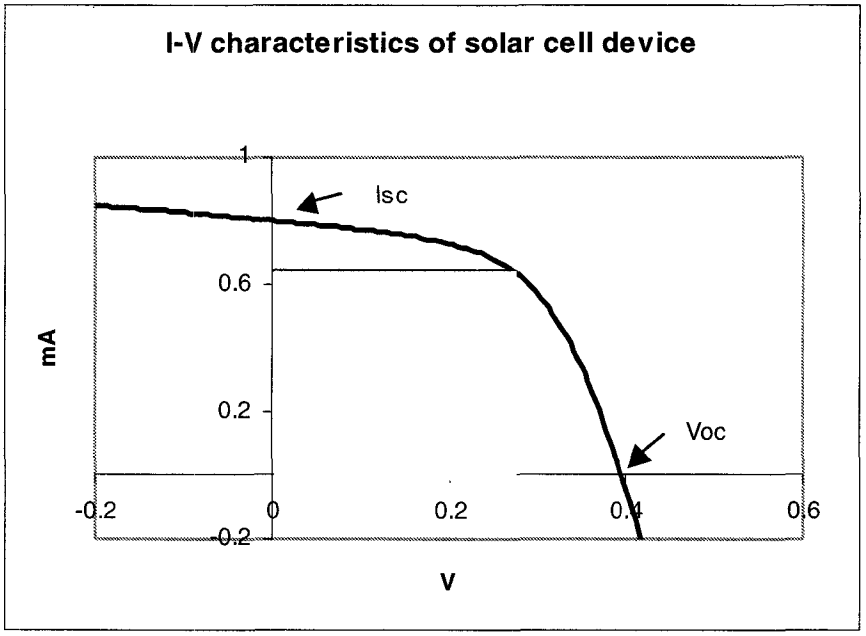

FIG. 3.4 a typical I-V curve of solar cell device

From the equivalent circuit model we discussed in chapter 2, the current-voltage of a solar cell can be written as:

$$I(V) = I_s\left[\exp\left(\frac{qV}{AkT}\right) - 1\right] - I_L(V)$$

where I_s is the saturation current of the diode; A is the diode factor. I_L is the photo generated current, also called short circuit current I_{sc}. It depends on the spectrum of the incident light and the collection efficiency. It can be written as following:

$$I_L = q\int(1-R)Q(E)S(E)dE$$

where R is the reflectance, S(E) is the spectrum of the incident light and Q(E) the collection efficiency of the solar cell.

The open circuit voltage, Voc, can be obtained from the previous two equations letting I(V) = 0. therefore we get

$$V_{oc} = \frac{AkT}{q} \ln\left(\frac{I_L}{I_s} + 1\right)$$

If we simplify the diode saturation current by

$$Is \approx \frac{qn_i W_d}{2\tau},$$

we can get

$$Voc \approx \frac{kT}{q} \ln\left(\frac{I_L}{I_s}\right) \approx \frac{kT}{q}\left[\ln(I_L) - \ln\left(\frac{qW_d}{2\tau}\sqrt{Nc \cdot Nv}\right)\right] + \frac{E_g}{2q}$$

Wd is the depletion width of the diode junction the n_i is the intrinsic carrier density. So the bandgap E_g is the most significant factor to change V_{oc}. Other factors affecting Voc include carrier lifetime, sample thickness and interface surface recombination rates etc.

Fill factor (FF) is the ratio of maxim power output to $I_{sc}V_{oc}$. This gives the real performance of the device used as a power source. High quality μc-Si solar cells can reach FF of 70% with V_{oc} of 0.5V or higher. The V_{oc} and FF are both functions of the material quality of the active layer of the cell, the interface properties and the engineering of the cell designing. Dangling bonds or other defects in the solar cell can trap and recombine the photo-generated carriers and greatly reduce V_{oc} and FF. Accidental doping in the active layer also decrease the lifetime of carriers and less carrier collection can be obtained.

Actual solar cell efficiency can be calculated by the ratio of maxim power output to the total illumination power.

- C-V characteristics

The n^+-n-p^+ can be approximated as a one-sided n-p^+ junction since the p+ doping is much higher then the doping in n layer. Most of the depletion region is in the lightly doped n-side.

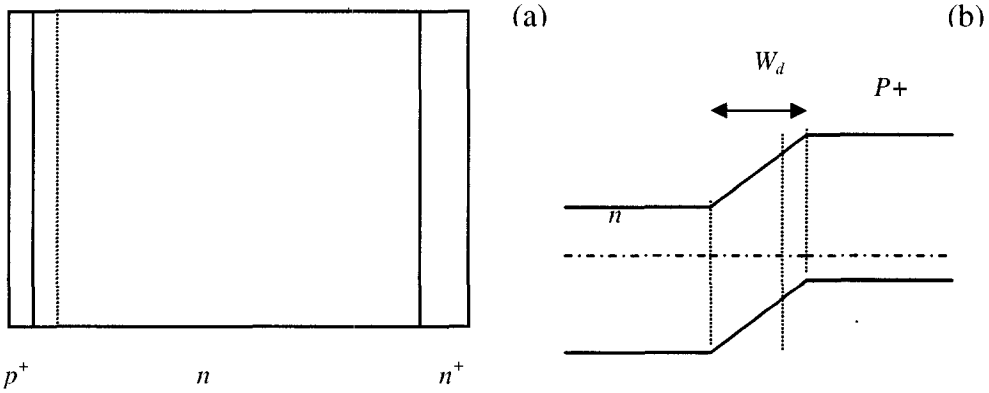

FIG. 3.5 (a) stucture schematic of a solar cell device; (b) the band diagram of the p+ layer and the n layer of the microcrystalline solar cell device

When a reverse bias is applied on the junction (negative voltage on the p+ side), the depletion width increases and the depletion capacitance decreases. By measuring the depletion capacitance, one can calculated the depletion width and the doping level by the following equations:

$$W_d = \frac{\varepsilon_s \cdot A}{C_d}$$

$$\frac{A}{C_d} = \sqrt{\frac{2(\psi_b + V_r)}{qN_d\varepsilon}}$$

In the measurement, a small ac signal of 100 Hz was superimposed on a DC voltage applied on the sample. It is notable that in amorphous materials, the band tail states which are deep below the conduction band do not respond to standard measurement frequencies unless extremely low frequency (as low as 10^{-4}Hz) or very high temperature is used. Since the μc-

SiGe bandgap is generally below 1.1 eV, the mid-gap deep state levels are only about 0.5 eV from the conduction band. A frequency of 100 Hz should be able to pick up all the defect and donar density [16].

According to Kimmerling Model, deep states give a different depletion width than shallow states even if they respond at the frequency of measurement, and low voltages pick up shallow states which are mainly donars. At high reverse voltages the deep state and shallow state depletion width approach each other and then gives both deep and shallow states.

- Quantum Efficiency (QE)

Quantum efficiency is defined as the ratio of number of collected carriers to the number of photons incident on the sample at a particular wavelength. It tells about how well the device absorbs photons at different wavelengths and how well the photo-generated carriers can transport through the device and get collected by the contact electrodes. The collection efficiency is reduced by the internal and surface recombination of carriers during the transport process. Also any problems in the device design that may inhibit collection of photo-generated carriers, such as hole trapping at the p-I interface, or the the valence band notch because of bandgap mismatching from amorphous silicon N+ layer to the active N layer, can be uncovered. From the QE dependence on the wavelength, such as the QE peak position, one can have an idea of the composition of the active layer.

A typical QE plot of μc-SiGe device is shown in Fig 3.5. the QE peak locates at 500-600 nm, which is close to a-SiGe device. But the long wavelength range QE values are significantly higher than in a-SiGe because of the greatly enhanced absorption in μc-SiGe.

Absolute QE can be estimated by using a laser (~620 nm) source setup as the illuminating light source. Comparing the current generated by the laser dot on the standard cell and the current on the sample cell, we can estimate the absolute QE.

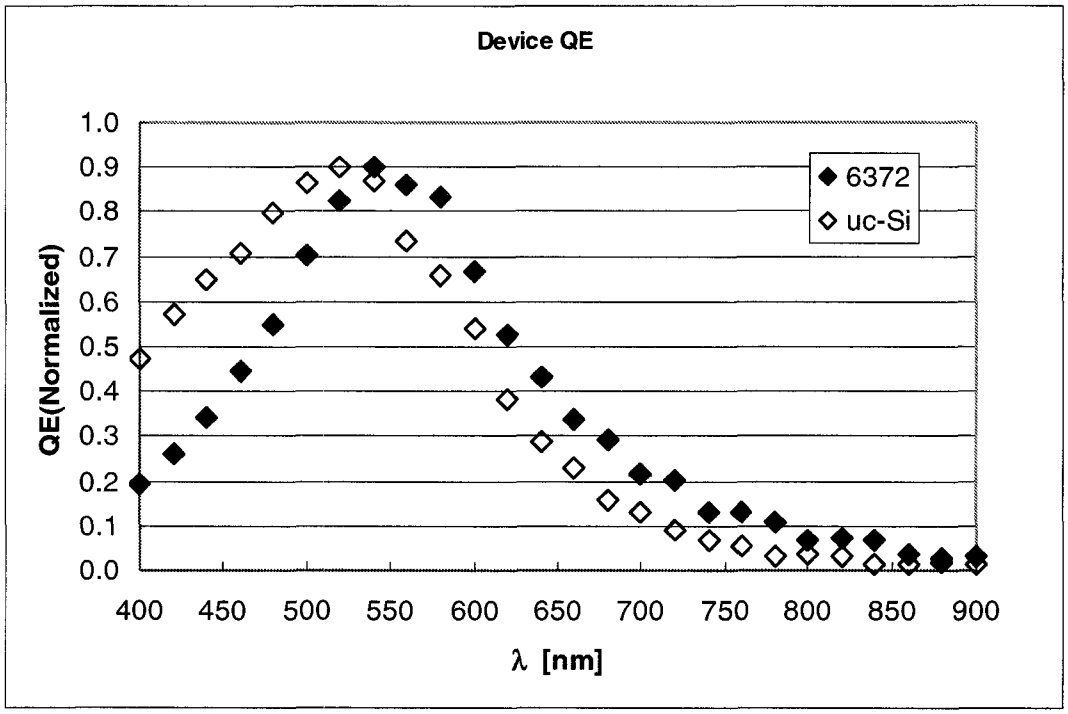

FIG. 3.6 QE of μc-SiGe device compared to μc-Si device showed enhancement of QE in the long wavelength range. The better QE of μc-Si device indicates the better p-i interface in μc-Si device

- Minority carrier diffusion length (L_p)

There have been several reports on the minority diffusion length measurement of microcrystalline materials and devices. Most well known of them are the Steady State Photocarrier Grating (SSPG) method for thin film samples [59] and Surface Photo Voltage (SPV) method for device samples [60]. However in the SPV method the sample was assumed to be infinitely thick. In this project a new method was developed for the estimation of minority carrier diffusion length in μc-SiGe p-i-n device.

The minority carrier diffusion length of μc-SiGe:H device was estimated by combining the reverse-biased C-V measurement and the QE measurement. Samples were measured using C-V at various reverse bias conditions and the depletion widths were calculated out.

A diagram of a solar cell under light shining is shown below. The quantum efficiency of the cell can be calculated by:

$$QE = \alpha W_d + \int_0^{t-W_d} \alpha(\lambda) e^{-\alpha x} e^{-\frac{x}{Lp}} dx = \alpha W_d + \frac{\alpha L_p}{1+\alpha L_p}\left[1 - e^{-\frac{t}{Lp}(1+\alpha Lp)}\right]$$

The first term is the collection in the depletion region by assuming all holes generated in the depletion region are swept to the p^+ contact and collected. The integral term is the QE of holes generated below the junction. If the thickness of the cell is much greater than the depletion width, which is usually the case in our samples, we can simplify the expression of QE by approximating the integral term:

$$QE = \alpha W_d + \frac{\alpha L_p}{1+\alpha L_p}$$

Experimental QE results are compared to this theoretical QE calculation to get the Lp values. Note this method is only a theoretical estimation of the minority diffusion length because of several reasons: (1) the thickness must be at least three times larger than the depletion width; (2) surface recombination is not considered in the calculation; (3) must use long wavelength photons to avoid the requirement for α which is usually unknown in the experiment. A typical L_p measurement plot is shown in Fig 3.7

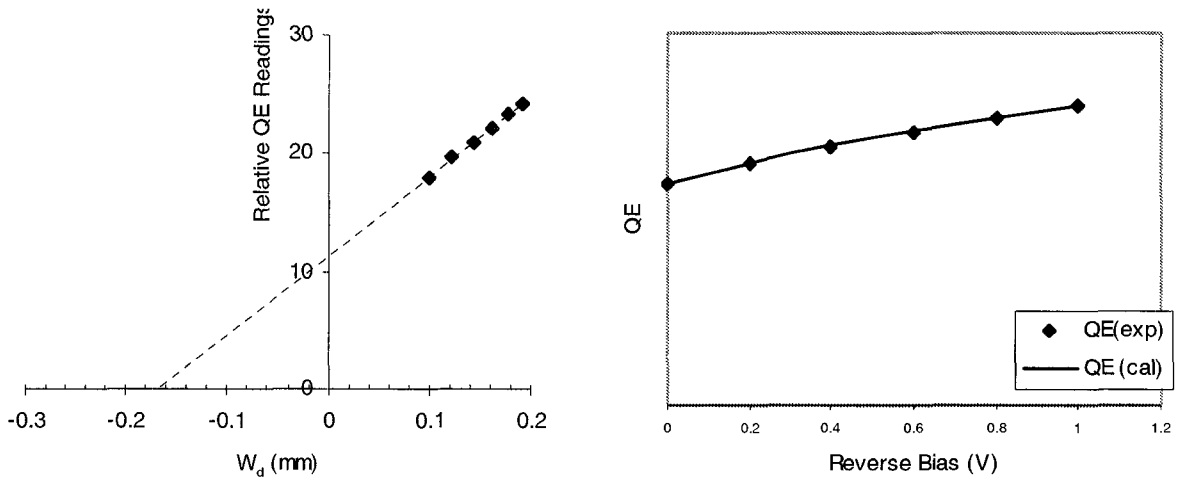

FIG. 3.7 Minority carrier diffusion length is measured from the QE (800 nm) change with reverse bias. The theoretical QE data calculated using this Lp value fit the experimental QE very well.

After the calculation of Lp we need to go back to the assumptions to see if all the assumptions are satisfied. If either of the assumptions is not met the calculation is not valid. Generally our device thickness are around 1.1 um while the Lp were measured to be less than 0.4 um. For most of the devices $Lp \ll t$ can be satisfied. If we use 800 nm QE data to estimate Lp, the $\alpha Lp \ll 1$ can also be satisfied.

CHAPTER 4. RESULTS AND DISCUSSIONS

4.1 Film Results

All the thin films samples are measured using the characterization methods discussed in chapter 3. These films are grown at 350 C using hydrogen plasma. The microwave power is kept 200W for all depositions and the thickness of the film samples are about 0.8 μm thick.

4.1.1 Ge concentration

μc-SiGe:H films of various Ge concentrations were deposited on glass substrates using ECR PECVD at different deposition conditions, such as different H_2 dilution rate R_H (R_H = $(SiH_4+GeH_4)/H_2$) and different GeH_4/SiH_4 flow ratios. Notice that to better control the SiH_4 and GeH_4 flow rates, 10% SiH_4 and 20% GeH_4 diluted in H_2 were used in the experiments. The H_2 from the SiH_4 and GeH_4 flows were included in the R_H and GeH_4/SiH_4 ratio calculations. The real Ge concentrations are calibrated by EDS measurement. The EDS results of samples deposited at different GeH_4/SiH_4 flow rates are shown in fig. 4.1. In the low Ge% region (< 20%), the actual Ge% is the same as the $GeH_4/(SiH_4+GeH_4)$ gas flow ratio. As more GeH_4 percentage in the source gas mixture, the Ge% becomes more than the GeH_4 ratio in the source gas. In the plot 60% GeH_4 actually produces over 70% Ge in the material. This can be explained from the different bonding energies between Si-H and Ge-H. The former bond has much higher bonding energy than the latter, and therefore more Ge related radicals are produced in the plasma and contribute to the film growth. Another possible reason of the higher Ge% is that the relatively heavier and easier to form Ge clusters in the volume and increases the Ge concentration.

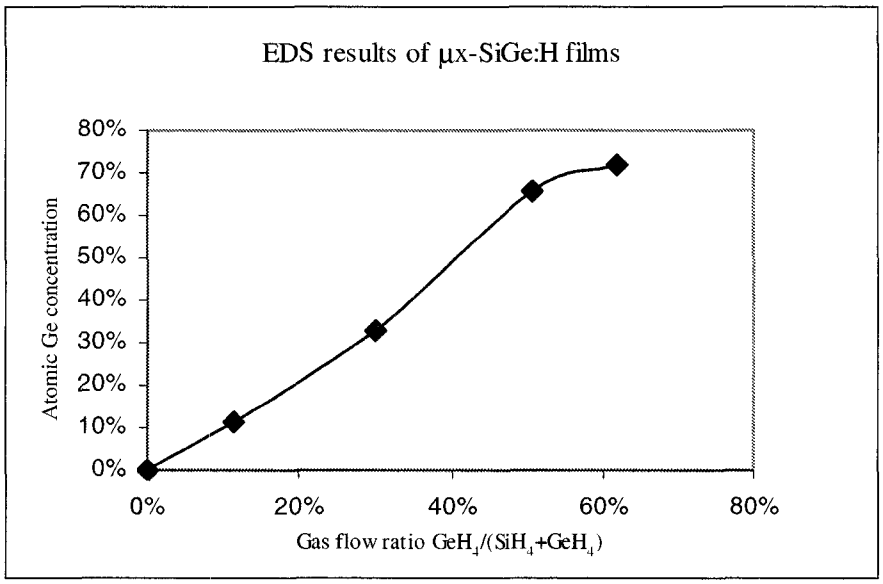

FIG. 4.1 EDS results of μc-SiGe:H films.

Table 4.1 briefly lists the films' deposition conditions and their optical properties. The activation energies are between 0.13 eV to 0.27 eV range, which is much lower than E_A of amorphous SiGe films as shown in ref [61]. Because E_A is basically the measure of difference between E_f and E_c, the increase of E_A with the GeH_4/SiH_4 ratio indicates less crystallinity with the incorporation of Ge into the material. This is confirmed by the UV reflection data shown in fig 4.2.

Table 4.1 Properties of μc-SiGe:H films at various deposition conditions

Sample #	GeH_4 (20%)	SiH_4 (10%)	GeH_4/SiH_4	E_a (eV)	E_{04} (eV)	σ_p/σ_d
5995	0	50	0.00	0.13	1.9	1.04
5996	5	50	0.13	0.16	1.93	1.81
5997	5	35	0.18	0.17	1.9	1.12
5983	5	25	0.26	0.19	1.87	2.72
5987	5	15	0.43	0.22	1.84	9.44
5989	8	15	0.69	0.22	1.73	5.70
6006	12	15	1.03	0.27	1.6	5.51
6029	12	12	1.29	0.27	1.5	1.80
6028	15	12	1.61	0.29	1.48	1.47

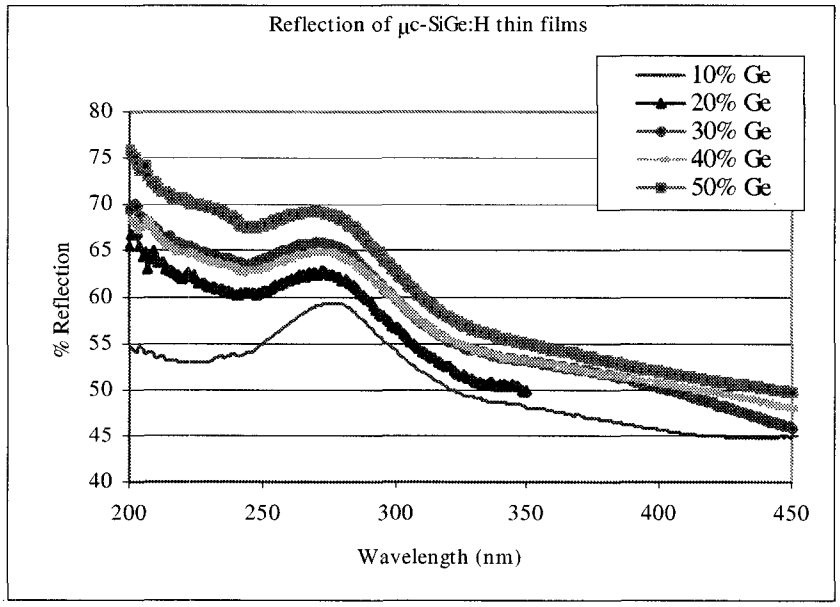

FIG. 4.2 The UV reflection curves of μc-SiGe:H films with different Ge%. The reflectance peak at about 270 nm is becoming flatter as the Ge% increases, indicating the worse crystallinity of the films.

The conductivities of μc-SiGe:H films are on the order of 10^{-6}-10^{-7} S/cm which are slightly lower than the 10^{-5} S/cm of μc-Si:H material, and the photosensitivity values are in the range of 1-10, and also much lower than the photosensitivities of amorphous SiGe films. Not that the electrical properties are affected not only by the Ge concentration but also by other factors such as crystallinity, grain size, impurity concentration and hydrogen content.

It is as expected that the optical absorption in long wavelength range is enhanced by increasing the Ge concentration. Fig 4.3 shows the different absorption curves of μc-SiGe:H film compared to the absorption of μc-Si films. With about 50% Ge incorporated, the μc-SiGe:H material shows about 10 times the absorption as in μc-Si material.

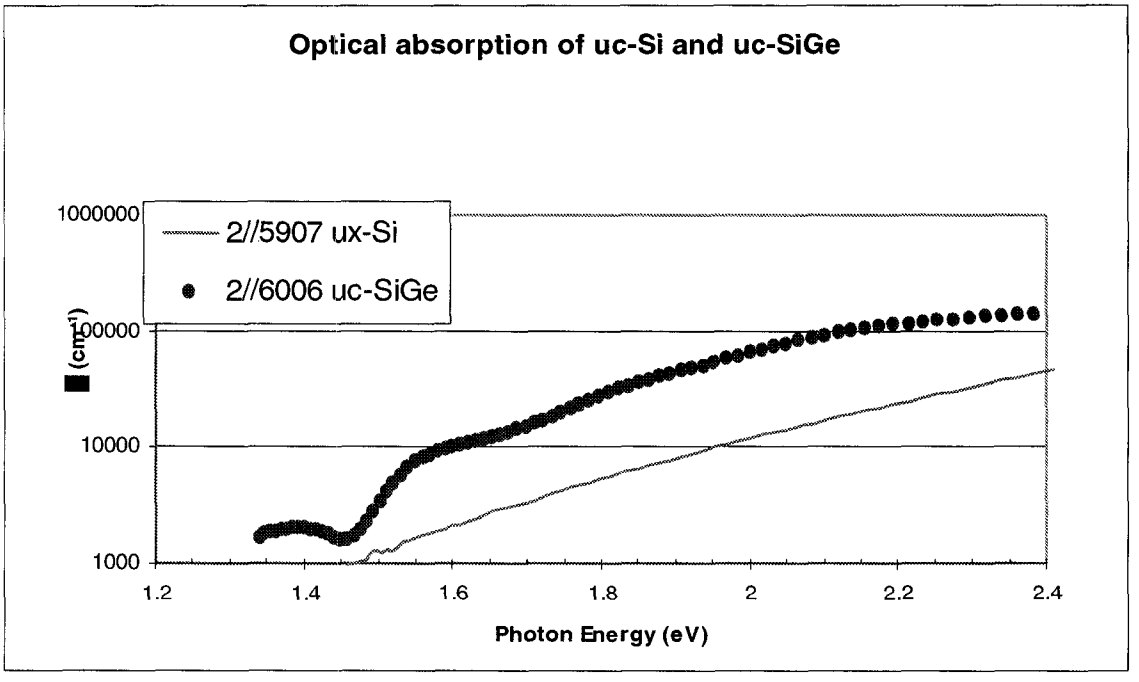

Fig. 4.3 Absorption curves of μc-SiGe films with about 50% Ge compared to the absorption of μc-Si thin films. It shows the enhanced absorption in μc-SiGe:H films than μc-Si:H in the whole range.

The optical bandgap shrinks with Ge%. Fig 4.4 shows the trend of E_{04} with relation to the GeH_4/SiH_4 flow ratio. The E_{04} badgap changes from about 2eV for μc-Si:H to below 1.5 eV for μc-SiGe:H with about 75% Ge incorporated.

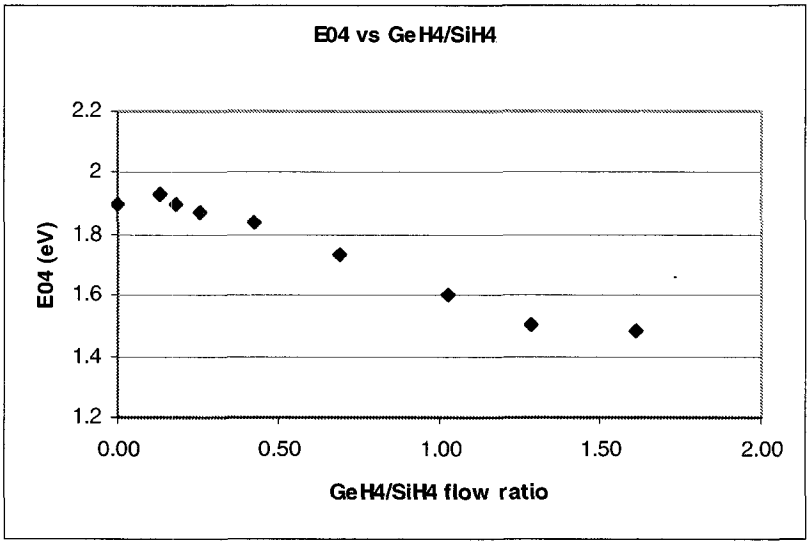

Fig. 4.4 Optical bandgap E04 of mc-SiGe:H films at different Ge concentrations. The bandgap shrinks almost linearly with Ge% in the material.

The Raman spectroscopy of μc-SiGe:H thin film is shown in fig. 4.5. The top Raman peak is sharp and located around 520 cm^{-1},which is the characteristic peak of crystalline Si. Because there is amorphous phase in the microcrystalline material, the Raman spectrum shows a bump at 480 cm^{-1}. As the Ge% increases, this Si-Si peak moves toward the lower wavenumber direction because the Si-Si bonds receive tensile and compressive stress due to the difference between the bond length of Si and Ge. For the same reason, the Ge-Ge peak moves toward higher wavenumbers as Ge% increases. The small bump at around 300 cm^{-1} locations is due to the amorphous phase of Ge clusters of small volume in the material. As the Ge% further increases, another peak at about 400 cm^{-1} becomes more and more dominant

and this peak is attributed to the Si-Ge bond in the material. At the same time we notice the Si-Si peak height decreases and further shifts toward the Si-Ge peak. In the 40% Ge spectra the Ge-Ge peak at 300 cm^{-1} becomes sharp, indicating long-term ordered Ge-Ge bonds are formed in the material structure. As the Ge concentration is increased to over 55%, the Si-Si peak disappears and the Ge-Ge bonds become the most dominant bonding configuration in the material.

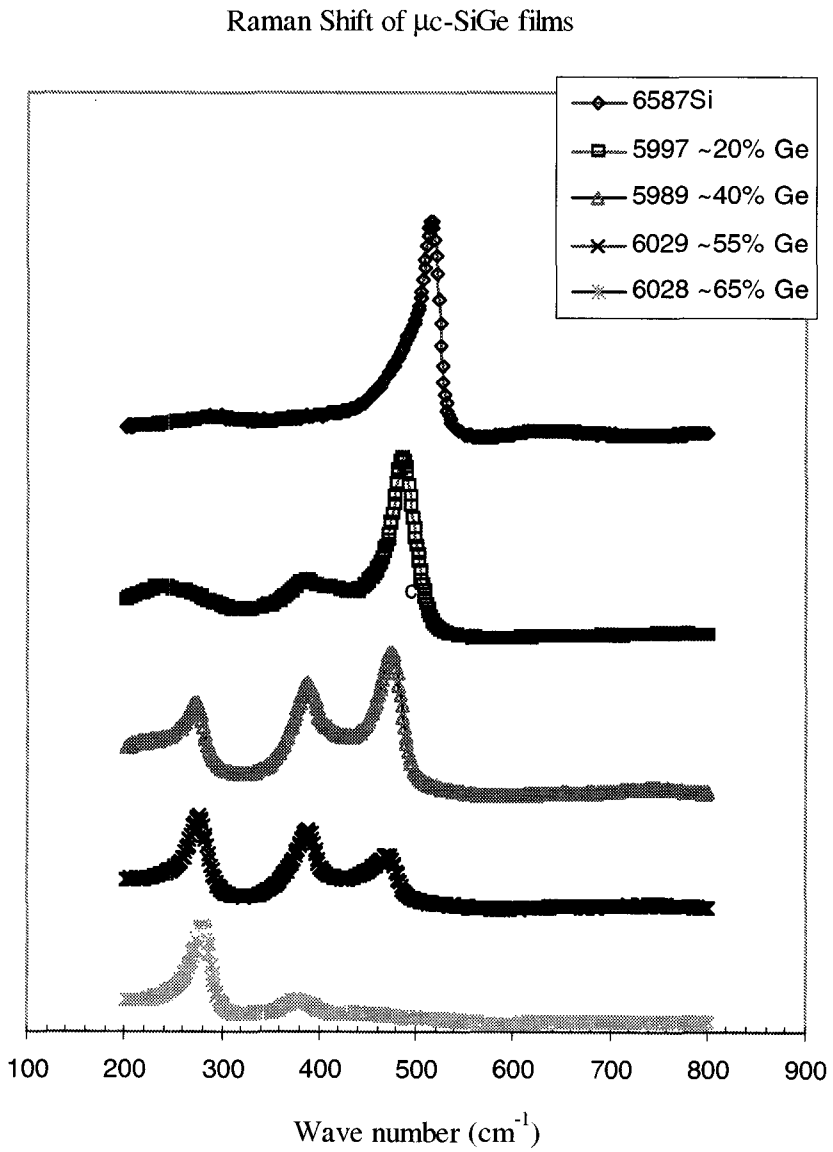

Fig. 4.5 Raman spectra of mc-SiGe:H thin films of various Ge concentration. The Si-Ge and Ge-Ge bondings become more and more dominant as the Ge concentration is increased in the material.

X-ray diffraction results shows (111) at 2θ ~ 28° is the dominant orientation of the crystals grown on stainless steel substrate. The two other XRD peaks at 47° and 55° can also be seen in the spectrum shown in fig 4.6. The grain size of the crystals is estimated ~100A from the (111) peak.

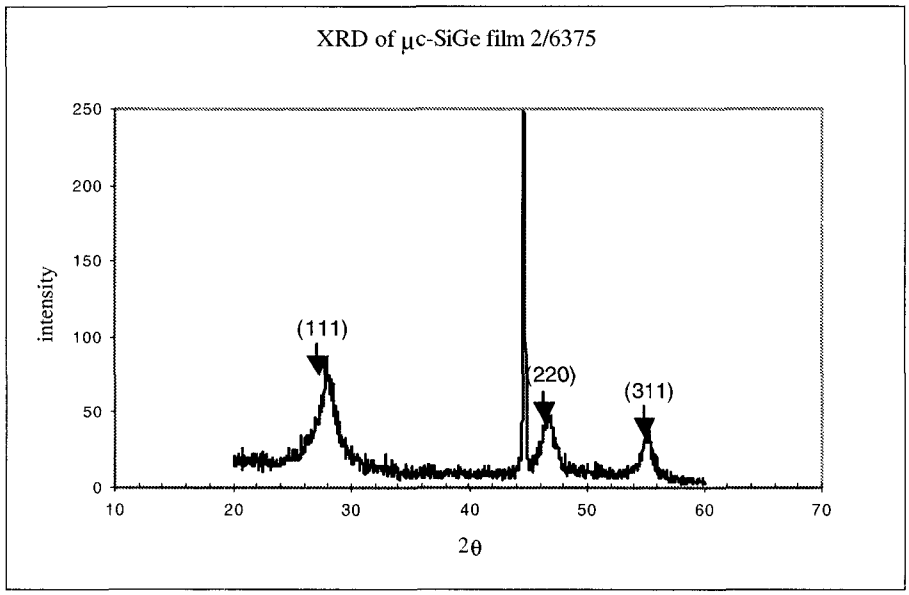

Fig. 4.6 X-ray diffraction spectrum of μc-SiGe:H thin film grown on stainless steel substrate. The dominant crystal orientation is (111).

4.1.2 H_2 dilution

The hydrogen dilution ratio is one of the most important deposition parameters for μc-SiGe:H growth. It has been confirmed by Raman spectroscopy in this project that high H2 dilution causes more crystalline material. As mentioned in chapter 1, some other groups obtained μc-SiGe:H material using RF PECVD deposition but at the extremely high H2 dilution rate (>100). It is shown in fig. 4.7 that high H_2 dilution rate causes reduced growth

rate for the μc-SiGe:H deposition. In this experiment by using ECR PECVD we achieved much higher growth rate at lower H_2 dilution rates than reported by other groups. The mc-SiGe:H films show microcrystalline properties even deposited at dilution rate as low as 1/15.

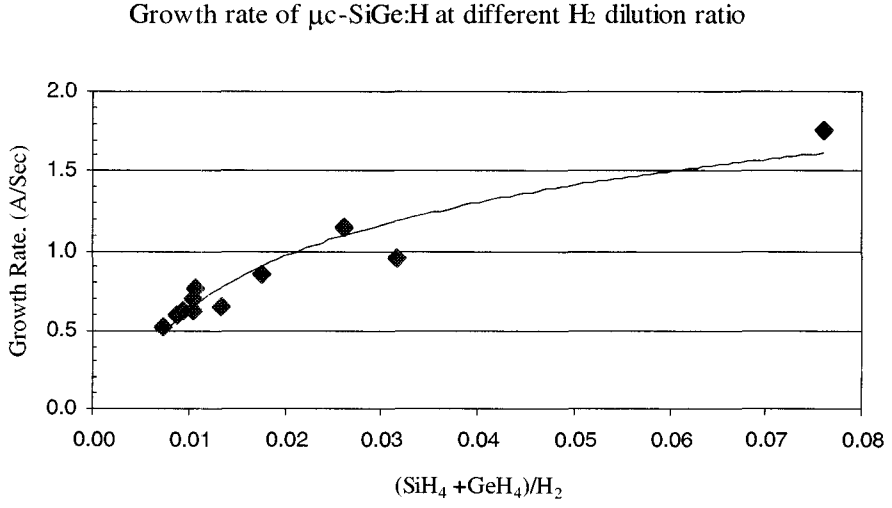

Fig. 4.7 Growth rate of mc-SiGe:H material at different H2 dilution rates. It is shown higher H2 dilution (lower SiH4+GeH4/H2) greatly reduces the deposition rate of mc-SiGe:H.

The effect of H2 dilution has been discussed by several groups for microcrystalline material. There are multiple roles of atomic hydrogen in the formation of μc-Si [62] as:

i. The hydrogen coverage of the growing surfaces enhances the diffusion of the adsorbed redicals as SiHx (x=1,2,3) [63]

ii. The weak Si-Si bonds at the growing surface are etched out by hydrogen radicals and crystallization takes place when chemical equilibrium between deposition and etching is attained.[64]

iii. Energetic atomic hydrogen penetrates into several layers below the top surface and promotes the network propagation reaction [65] by (a) dangling bond

compensation, (b) weak bond breaking and reconstruction of strong Si-Si bonds, (c) strain relaxation, and (d) giving chemical potential to the growing surface by breaking the Si-H bond which is an exothermic process, thereby leading to structural reorientation for attaining energetically favorable configuration and hence microcrystallization.

In our μc-SiGe:H case, the role of hydrogen dilution is even more complicated because more types of radicals are involved during the process. Generally the hydrogen coverage on the surface enhances the diffusion of the film forming precursors and helps to reach the energetically favorable sites. Hence the resulting film is homogeneous containing less active defects. This is especially important for the diffusion of Ge radicals because of they are heavier than Si radicals. This is why a higher H2 dilution rate is required for the crystallization of μc-SiGe alloy. The growth rate data indicates the hydrogen radical assisted etching of the amorphous part also helps in the formation of microcrystalliation.

In our experiments of device deposition, a high hydrogen dilution ratio was used in the μc-Si buffer layer to increase the nuclei density and initiate the crystallinzation. To grow a microcrystalline layer on a foreign substrate requires a neucleation process prior to the real growth. It has been reported for μc-Si:H grown on glass substrate or on other amorphous substrate such as a-Si:H included a necessary incubation amorphous silicon layer of about 100A before the onset of microcrystalline growth. In our experiment this incubation layer is also observed for μc-SiGe:H samples grown on amorphous silicon and on glass substrates. This incubation amorphous layer can impact both the film properties and the performance of solar cell devices using a-Si in the n^+ layer. To improve the crystallinity of the active layer in μc-SiGe:H device in our experiment, a thin μc-Si "buffer" layer is deposited on the a-Si n+

layer prior to the deposition of the real μc-SiGe layer. There are several reasons for this and results have shown the advantages on both the material growth and the carrier transport. This issue will be discussed in detail. As soon as the crystallization is initiated, the high hydrogen dilution ratio is no longer required. We start the real μc-SiGe growth on top of these crystallized sites and the crystallinity can still be maintained at hydrogen dilution ratio as low as 1:15.

4.2 Device Results

Devices are prepared using Phosphors doped a-Si layer as the n^+ layer grown on stainless steel substrates. The thickness of this n+ layer is about 0.1 μm. μc-SiGe:H is the active layer of the devices and it is deposited on top of the n+ layer. Since the n+ layer is also deposited in the same chamber as the active layer, a lot of purging and evacuation steps are needed between the deposition of these two layers and an over one hour dummy layer grow a thick and hard SiC layer on the chamber surface with the shutter closed to cover the residual dopant atoms and prevent them from coming into the devices. The experiment calibrated the growth rate of each set of deposition process before using the parameters for device growing so that the thickness of all devices are controlled to be close to 1.0 μm. As mentioned before, all the devices used a thin μc-Si buffer layer between n and the real μc-SiGe active layer. The main purpose is to complete the nucleation and initiate the crystallinization in this buffer layer and hence we could decrease the hydrogen dilution in the following real active μc-SiGe:H layer. It has been confirmed by the device performance that this buffer layer is extremely important both for the crystallinity of μc-SiGe:H in the device but also for the device engineering itself such as shunting the possible shorts on the substrate.

For most of the μc-SiGe:H solar cell devices a fill factor over 55% was achieved. A I-V curve of a μc_SiGe:H device with 40% Ge is shown in fig. 4.8.

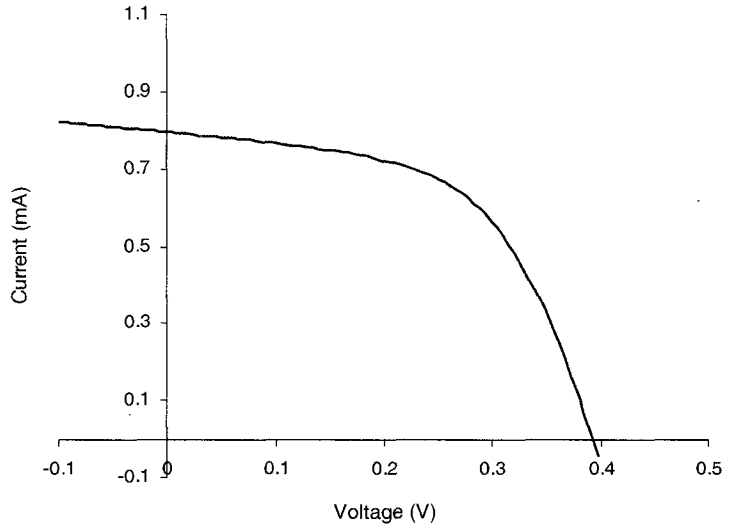

FIG.4.8. I-V characteristics of a μc-SiGe device with 40% Ge. It shows Voc of 0.393 V and FF of 57%.

4.2.1 Devices with various Ge concentration

It has been discussed in the previous sub chapter that the bandgap of μc-SiGe material shrinks with the Ge concentration. As shown in fig. 4.9, Voc and FF also decreases with the Ge concentration in the active layer of the cell. The decrease of Voc is mainly due to the decrease of the material bandgap of the active μc-SiGe:H layer with increasing Ge concentration. The defects created by the Ge atoms in the material also caused the decrease of Voc. The reducing FF indicates the worse transport of photo-generated carriers in the device. For the cells with less than 35% of Ge incorporated, the FF are over 55%, and this is a good achievement for μc-SiGe:H solar cell devices, which may suggest ECR PECVD is a better choice than regular RF PECVD technique. Also worth to note is that the H_2 dilution rates used in the growth of all devices are in the range of 1:20 to 1:50, much lower than

reported by other groups using RF PECVD technique, and therefore much higher deposition rates were obtained in this projects. The advantages of using ECR PECVD may come from the high density and low ion energy features. The high density plasma may have enhanced the growth rate while the ions with relatively low energy bring less bombardment to the growth surface and cause less defects in the material.

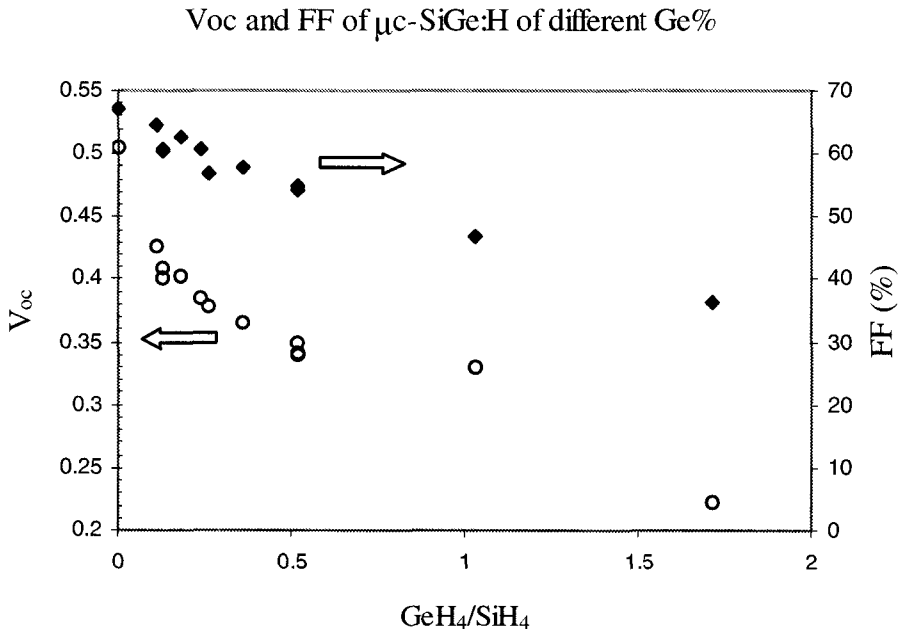

FIG. 4.9 The change of Voc and FF with different GeH4/SiH4 flow ratio in the mixture source gas.

In fig. 4.10 the device normalized QE is plotted for different Ge concentrations. The curve on the bottom of the plot is the QE of a μc-Si device for comparison. The QE of μc-SiGe:H cell is much higher in the longer wavelength range than μc-Si device. The long wavelength (low photon energy) QE values shift higher for devices with more Ge%. The QE at 800 nm was plotted for a better comparison in fig. 4.11.

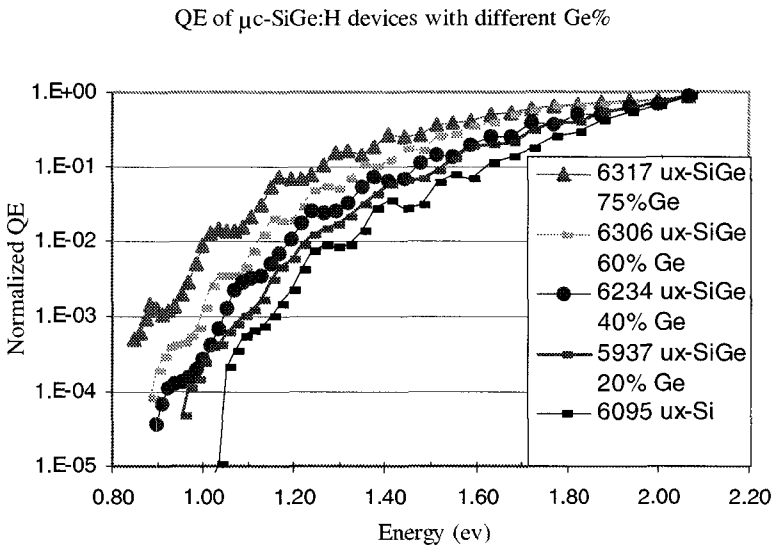

FIG. 4.10 Quantum Efficiency of μc-SiGe:H devices with different Ge concentration.

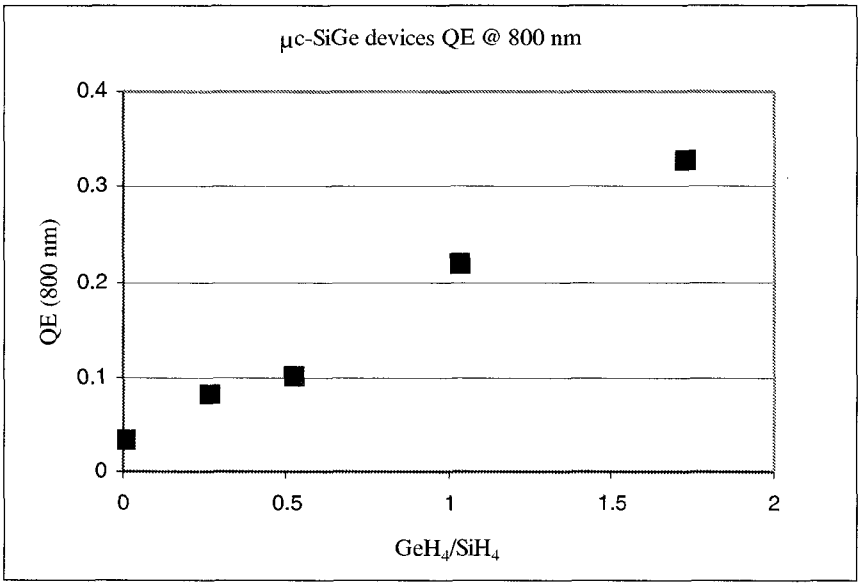

FIG. 4.11 The comparison of device QE at 800 nm shows increase of QE with the Ge concentration in the active μc-SiGe:H layer.

4.2.2 μc-Si buffer layer effect on μc-SiGe:H device

The μc-Si buffer layer was grown on top of the n+ layer before the growth of real μc-SiGe active layer. This design of the device turned out to be very beneficial to the solar cell performance. Fig 4.12 shows the different device I-V characteristics of two devices with and without this μc-Si buffer layer. The device with μc-Si buffer layer shows much better performance than the sample without buffer layer in all aspects including Voc, Isc and FF.

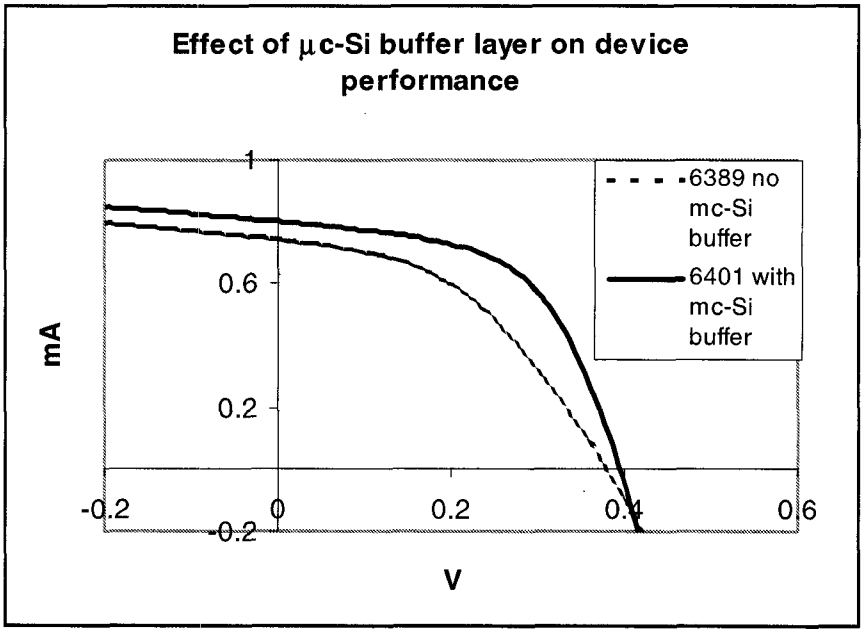

FIG 4.12 μc-Si buffer layer effect on μc-SiGe device performance. The device with the buffer shows much better performance than the one without buffer layer.

The different behaviors of device with and without μc-Si buffer between n+ and active n layer can be understood in two aspects. First, during the sample growth, because of the higher hydrogen dilution rate in this buffer layer, the thin μc-Si buffer layer completes the necessary nucleation and initiate the crystallization process. Therefore the μc-SiGe layer was actually grown on a crystallized surface instead of on the amorphous n+ layer. This microcrystallized surface fastened the crystallization in the μc-SiGe and improved the

microstructure. Also importantly is that the hydrogen dilution rate can be lowered down significantly after the nucleation completed in the buffer layer, and the actual growth rate in the μc-SiGe can be greatly increased by decreasing the hydrogen while keeping good crystallinity in the material. Constantly good devices were successfully made by this means at a relatively higher growth rate. Secondly, this buffer layer actually started with a thin incubation layer from the amorphous n+ layer and passivated the shorts on the substrate and hence increased the shunt resistance of the device. In this way the performance of the solar cell device could also be greatly improved.

4.2.3 Carrier transport in devices

All μc-SiGe devices with 30% were selected to investigate the carrier transport. The device properties are listed in Table 4.2. The total device thickness is about 1.1 μm. Doping levels in these devices were intentionally changed by including different amount of ppm level TMB into the source gas mixture during the deposition process. The H2 dilution rate was maintained at 1:25 and μc-Si buffer layer is used between n+ and μc-SiGe:H layers. Deposition temperature is kept at 350 °C for the μc-SiGe:H layer in the devices.

The results showed Voc's in the range of 0.37 to 0.39 V and FF about 45% to 57%. Since there is no Ge% or H2 dilution change between these devices, the different cell performances can only be attributed to the different carrier transport. The change of QE at 800 nm also confirms the different carrier transport in these devices.

Table 4.2 Results of μc-SiGe devices with 30% Ge

sample #	t (um)	Voc(V)	Isc(mA)	FF(%)	QE (800nm)	Nd (cm^{-3})
6372	1.08	0.377	0.797	55.1	0.066	2.08E+17
6373	1.06	0.388	0.84	50	0.077	1.66E+17
6374	1.04	0.373	1.18	51.6	0.119	6.95E+16
6376	1.06	0.392	0.995	51.7	0.068	1.08E+17
6379	1.05	0.388	0.691	56.6	0.08	3.07E+17
6380	1.11	0.387	0.81	55.2	0.105	2.09E+17
6384	1.14	0.398	0.851	52.3	0.066	1.44E+17
6389	1.08	0.381	0.742	44.7	0.0745	1.56E+17
6401	1.2	0.395	0.799	57	0.067	1.74E+17
6412	1.16	0.388	0.981	55.6	0.079	9.70E+16
6413	1.15	0.397	0.877	55.7	0.073	1.30E+17
6414	1.1	0.38	0.987	55.2	0.092	7.27E+16
6415	1.19	0.372	1.13	52.9	0.105	5.51E+16

C-V measurements show that the doping levels are significantly different in the n layers of the devices, ranging from 5E16/cm^3 to over 3E17/cm^3. Fig 4.13 is plotting the doping level in the n layer with the TMB flow rate during the deposition of μc-SiGe:H layer. More TMB can compensate the accidental O doping in the deposition process and decrease the doping level in device.

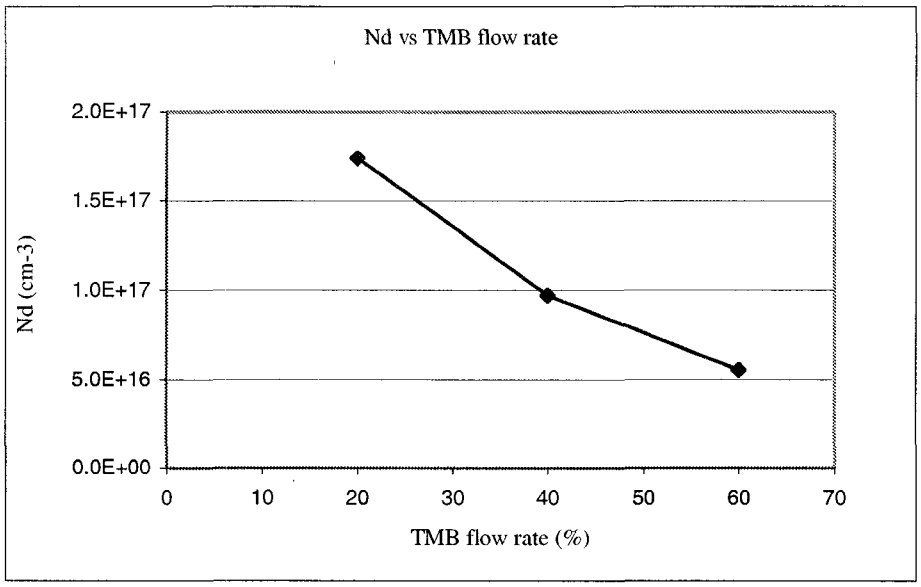

FIG. 4.13 Doping level in μc-SiGe n layer decreases with TMB flow rate suring deposition.

Fig. 4.14 shows the relation between short circuit current and the TMB flow rate. By increasing the TMB flow rate from 20% to 60%, the sort circuit current increased by about 40%. This is a significant change since the output power of solar cell is directly related to how much current the cell provides to the load.

Table 4.3 μc-SiGe device Nd and Lp results

sample #	Nd	Lp
6372	2.08E+17	0.13
6374	6.95E+16	0.3
6376	1.08E+17	0.21
6401	1.74E+17	0.17
6413	1.30E+17	0.21
6414	7.27E+16	0.3
6415	5.51E+16	0.38

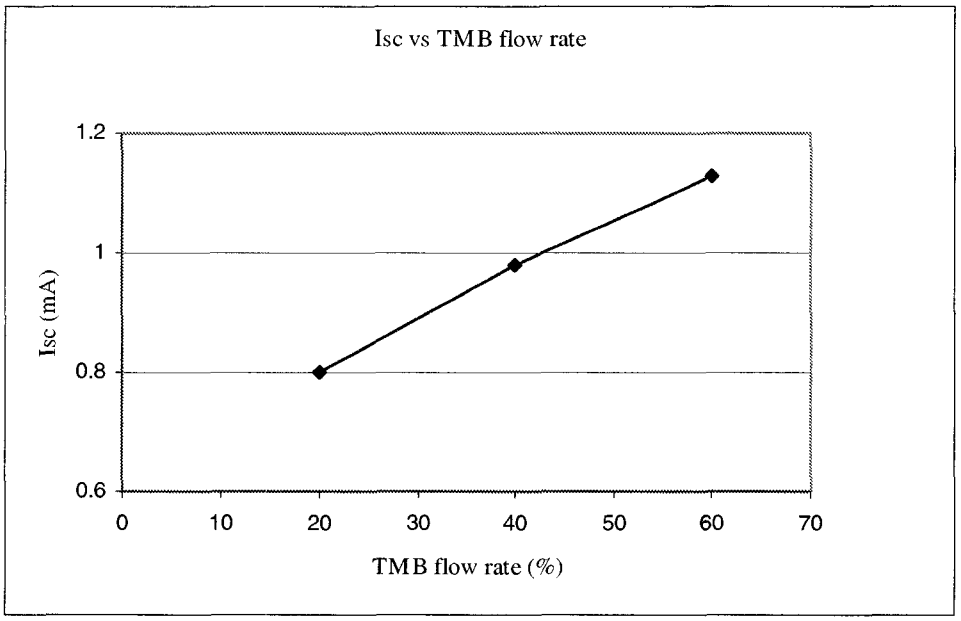

FIG. 4.14 Short circuit current with TMB flow rates

The minority carrier (hole) diffusion length was estimated by the combined QE and C-V method described in the previous chapter. A summary of the Lp results is shown in table 4.3.

As shown in fig 4.15, minority carrier diffusion length of the cells increased from 0.13 μm to 0.38 μm while the doping level dropped from over 2E17cm^{-3} to 5.5E16cm^{-3}. The decrease of L_p with increasing N_d suggests more recombination centers are created by the accidental oxygen doping in the devices. The oxygen doping can affect the hole diffusion by two means: 1) the defect produced by the oxygen atoms can be an effective recombination center for holes; 2) the increased electron density in the material decrease the hole lifetime.

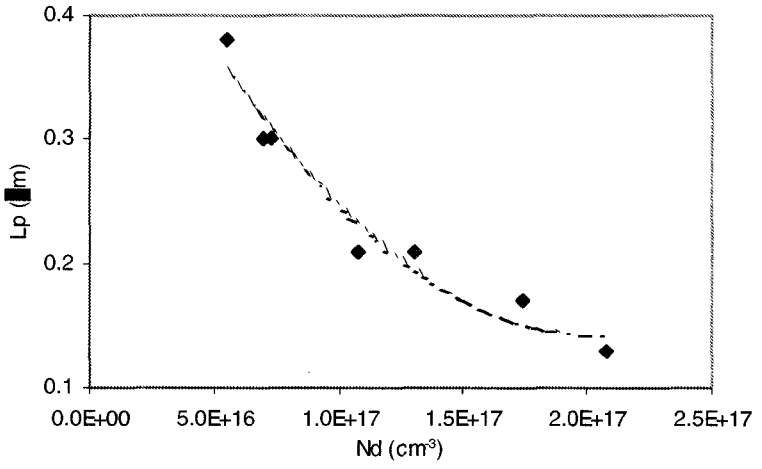

FIG. 4.15 Increased doping in the n layer reduces the diffusion length of minority carrier.

CHAPTER 5 SUMMARIES AND CONCLUSIONS

Although there have been a lot of work accomplished or on going for μc-Si:H, there was very few reports on μc-SiGe:H material. The main reason is the difficulty to obtain μc-SiGe:H samples of good quality at reasonable growth rates. In this work, a different growth technique - ECR PECVD is used to deposit μc-SiGe:H material using hydrogen plasma. It is found that the growth rate can be greatly enhanced by taking advantage of the high plasma density and low ion energy features of ECR and extremely high hydrogen dilution ratios are no longer necessary for μc-SiGe:H growth. Films with good crystallinity can still be obtained at hydrogen dilution ratio as low as 1:15. This is very encouraging for the commercialization of μc-SiGe:H solar cell devices.

For the first time ever, an intensive study has been completed for the μc-SiGe:H with a full Ge% range. EDS shows the actual Ge concentration is higher than the GeH_4 percentage in the source gas mixture. The optical bandgap shrinks with the incorporation of Ge into the material. The increase of activation energy and photosensitivity indicates the deterioration of crystallinity by bringing Ge to the Si struture and this has been confirmed by Raman spectra.

Solar cell devices using μc-SiGe:H as the active layer were deposited on stainless steel substrates. Fill factors over 55% were achieved for μc-SiGe devices with less than 35% Ge. As in amorphous silicon germanium, the device performance deteriorates as more Ge is incorporated. An buffer layer between n+ and μc-SiGe:H n layer was used in the device design and this buffer layer revealed to be very beneficial to the device performance because the neucleation process is completed in this buffer layer and the real growth of μc-SiGe:H on top of crystallized Si layer is greatly fastened.

Measurement of fundamental material properties in devices such as donor density, deep defect density and diffusion lengths of minority carriers were completed for the first time ever in microcrystalline solar cell system. C-V measurements were used in this project to discover the doping levels in the active n layer of the devices. It is found that the accidental oxygen leakage can raise the doping level to the order of 1E17cm^{-3}. ppm level TMB can be mixed in the source gas to very effectively reduce the N-type doping brought by oxygen. Short circuit current can be increased by the TMB counter doping.

The minority carrier diffusion length was estimated from reversed bias QE and C-V measurements. In the μc-SiGe:H devices fabricated by ECR PECVD, the hole diffusion length is several tenth micrometers. The transport of photo-generated carriers in the solar cell devices are investigated in this project and it is found that accidental doping in the μc-SiGe:H deteriorates the device performance by decreasing the minority carrier diffusion length. Compensating doping of TMB can increase L_p and improve short circuit current, and hence improve the conversion efficiency of solar cell device.

In summary, this project has succeeded in making good quality μc-SiGe:H material and solar cell devices of various Ge concentrations at improved deposition rate using ECR PECVD technique. Carrier transport was studied in the devices and accidental doping plays a key role in microcrystalline device performance.

REFERENCES

[1] D. L. Staebler and C. R. Wronski, "Reversible conductivity changes in discharge-produced amorphous Si", Appl. Phys. Lett., Vol. 31, p.292, 1997.

[2] J. Meier, et al., Mater. Res. Symp. Proc., Vol.3, p.420, 1996.

[3] K. Yamamoto, et al., Technical Digest of the International PVSEC-11, p.225, 1999.

[4] K. Yomomoto, et al., Proceedings of the Second World Conference Photovoltaic Energy Conversion, p.1284, 1998.

[5] D. E. Carlson, L. F. Chen, G. Ganguly, G. Lin, A. R. Middya, R. S. Crandall, and R. Reedy, MRS Spring Meeting, San Francisco, 1999.

[6] F. Siebke, S. Yaha, Y. Hishikawa, and M. Tanaka, J. Non-Cryat. Solids, 977, 227-230 (1998).

[7] A. Gross, O. Vetterl, A. Lambertz, F. Finger, H. Wagner, and A. Dasgupta, N-side illuminated microcrystalline silicon solar cells, Applied Physics Letters, Vol. 79, No. 17, 2001.

[8] I. Sieber, I. Urban, I. Dorfel, S. Koynov, R. Schwarz, and M. Schmidt, Thin Solid Films Vol. 276, p.314, 1996.

[9] L. L. Smith, E. Srinivasan, and G. N. Parsons, J. Appl. Phys. Vol.82, P.6041, 1997.

[10] E. Srinivansan and G. N. Parsons, J. Appl. Phys. 81, 2847 (1997).

[11] B. Rezek, J. Stuchlik, A. Fejfar, and J. Kocka, Appl. Phys. Lett. 74, 1475 (1999).

[12] C. Ross, J. Herion, and H. Wagner, J. Non-Cryst. Solids 266-269, 69 (2000).

[13] K. Bruhne, S. Klein, and M. B. Schubert, in Proceedings of the 16th European Photovolt. Solid Energy Conference, Glasgow, 2000 (James and James, London, 2000), VB 1.17.

[14] L. Houben, M. Luysberg, P. Hapke, R. Carius, F. Finger, and H. Wagner, Philos. Mag. A 77, 1447 (1998).

[15] E. Vallat-Sauvain, U. Kroll, J. Meier, N. Wyrsch, and A. Shah, J. Non-Cryst. Solids 266-269, 125 (2000).

[16] V. L. Dalal, J. H. Zhu, M. Welsh and M. Noack, Microcrystalline Si:H solar cells fabricated using ECR plasma deposition, IEE, 2003.

[17] J. K. Rath, F. D. Tichelaar, H. Meiling, and R. E. I. Schropp, Amorphous and Microcrystalline Silicon Technology-1998, edited by S. Wagner, m. Hack, H. M. Branz, R. Schropp, and I. Shimizu, Mater. Res. Soc. Symp. Proc. 507 (Materials Research Society, Pittsburgh, 1999).

[18] P. Brogueira, V. Chu, and J. P. Conde, Amorphous and Heterogeneous Silicon Thin Films: Fundamentals to Devces-1999, edited by H. M. Branz, R. W. Collins, H. Okamoto S. Guha, and R. Schropp, Mater. Res. Soc. Symp. Proc. 557 (Materials Research Society, Pittsburgh, 1999).

[19] P. Roca I Cabarrocas, N. Layadi, T. Heitz, B. Drevillon, and I. Solomon, Substrate selectivity in the formation of microcrystalline silicon: Mechanisms and technological consequences, Appl. Phys. Lett. 66 (26), 1995.

[20] S. Mukhuopadhyay, S. Saha and S. Ray, Role of Substrate Temperature on the Properties of Microcrystalline Silicon Thin Films, Jpn. J. Appl. Phys. Vol. 40 (2001) pp. 6284-6289.

[21] S. Ray, C. Das, S. Mukhopadhyay, S.C. Saha, Substrate temperature and hydrogen dilution: parameters from amorphous to microcrystalline phase transition in silicon thin films, Solar Energy Materials & Solar Cells (2002).

[22] C. C. Tsai, R. Thompson, C. Doland, F. A. Ponce, G.B. Anderson, and B. Wacker, Mater. Res. Soc. Symp. Proc. 118, 49 (1988).

[23] J. S. Chou, W. J. Sah, S.C.Lee, T.C.Chang, and J.C.Wang, Mater. Chem. Phys. 32, 273, (1992).

[24] A. Matsuda, J. Non-Cryst. Soilids 59& 60, 767 (1983).

[25] O. Vetterl, F. Finger, R. Carius, P. Hapke, L. Houben, O. Kluth, A. Lambertz, A. Muck, B Rech, and H. Wagner, Sol. Energy Mater. Sol. Cells 62, 97 (2000).

[26] Hiroyuki Fujiwara, Michio Kondo, and Akihisa Matsuda, Real-time Spectroscopic ellipsometry studies of the nucleation and grain growth process in microcrystalline silicon thin films, Physical Review B, Vol. 63, The American Physical Society, 2001.

[27] S. veprek, A. Iqbal, H. R. Ostwald, and A. P. Webb, J. Phys. C 14, 295 (1981).

[28] A. Matsuda and K. Tanka, J. Non-Cryst. Solids 97, 1367 (1987).

[29] A. Matsuda, J. Non-Cryst. Solids 59, 767 (1983).

[30] K. Saitoh, M. Kondo, M. Fukawa, T. nishmiya, W. Futako, I. Shimizu, and A. Matsuda, Mater. Res. Soc. Symp. Proc. 507, 843 (1999).

[31] M. Kondo, M. Fukawa, L. Guo, and A. Matsuda, J. Non-Cryst. Solids 266, 84 (2000).

[32] M. Nakata, A. Sakai, T. Uematsu, T. Namikawa, H. Shirai, J. Hanna, and I. Shimizu, Philos. Mag. B 63, 87 (1991).

[33] H. Shirai, D. Das, J. Hanna, and I. Shimizu, Appl. Phys. Lett. 59, 1096 (1991).

[34] K. Nakamura, K. Yoshino, S. Takeoka, and I. Shimizu, Jpn. J. Appl. Phys., Part 1 34, 442 (1995).

[35] S. Sriraman, S. Agarwal, E. S. Aydil, and D. Maroudas, Nature (London) 418, 62 (2002).

[36] P. R. I. Cabarrocas, S. Hamma, A. Hadjadj, J. Bertomeu, and J. Andreu, Appl. Phys. Lett. 69, 529 (1996).

[37] A. F. I. Morral, J. Bertomeu, and P. R. I. Cabarrocas, Mater, Sci. Eng., B 69, 559 (2000).

[38] J. Robertson, Thermodynamc model of nucleation and growth of plasmas deposited microcrystalline silicon, Journal of Applied Physics, Vol. 93, No. 1, 2003.

[39] B. Kalache, A.I. Kosarev, R. Vanderhaghen, and P. R. I. Cabarrocas, Ion bombardment effects on microcrystalline silicon growth mechanisms and on the flim properties, Journal of Applied physics, Vol. 93, No. 2, 2003.

[40] G. Ganguly, T. Ikeda, T. Nishimiya, K. Saitoh, M. Kondo, and A. Matsuda, Hydrogenated microcrystalline silicon germanium: A bottom cell material for amorphous silicon-based tandem solar cells, Apppl. Phys. Lett. 69 (27), 1996.

[41] V. L. Dalal and K. Erickson, Microncrystalline Si and (Si, Ge) Solar Cells on Plastic Substrates, IEEE, 2000.

[42] Shaoyun Huang, Kunji Chen, Jianjun Shi, Xinfan Huang, Jun Xu, Gautam Ganguly and Akihisa Matsuda, Very high hydrogen dilution induced novel phenomena of electronic transport properties in hydrogenated microcrystalline Silicon-Germanium thin films, Jpn. J. Appl. Phys. Vol. 40 (2001) pp. 40-43

[43] Jatindra K. Rath, F. D. Tichelaar, Ruud E. I. Schropp, Heterogeneous growth of microcrystalline silicon germanium, Sloar Energy Materials & Solar Cells, 2002.

[44] V. L. Dalal, S. Kaushal, and J. Xu, Growth of high quality a (Si, Ge): H films using low pressure remote ECR Discharge, J. Non-Cryst. Solids, 1996, 198-200, p. 563.

[45] V. L. Dalal, M. Pontoh, and N. Gandhi, Characterization of ECR plasma, Proc. Mater. Res. Soc., 2002, 715.

[46] V. L. Dalal, S. Haroon, Z. Zhou, T. Maxson and K. Han, Influency of Plasma Chemistry on the properties of a- (Si, Ge): H Alloys, Journal of Non-Crystalline Solids, 266-269(1-3), 675 (2000).

[47] V. L. Dala, T. Maxson, And S. Haroon, Influence of Plasma Chemistry on the Properties of Amorphous (Si, Ge) Alloy Devices, Mat. Res. Soc. Symp. Proc. , 507, 441 (1998).

[48] V. L. Dalal, Some Considerations Relating to Growth Chemistry of Amorphous Si and (Si, Ge) Films and Devices, Mat. Res. Soc. Sym. Proc. 664, A5. 2 (2001).

[49] V. L. Dalal, Fundamental Considerations regarding the Growth of Amorphous and Microcrystalline Silicon and Alloy Films, J. Non-Cryst. Solids, 395, 173 (2000).

[50] W. Luft and Y. Tsuo, Hydrogenated Amorphous Silicon Alloy Deposition Processes, Marcel Dekker, Inc., New York (1993).

[51] J. J. Wagner and S. Veprek, Plasma Chem. Plasma Proc. 2, 95(1982).

[52] C.C. Tsai, G. B. Anderson, R. Thompson, and B. Wacker, J. Non-Cryst. Solids, 114, 151 (1989).

[53] I. Solomon, B. Drevillon, H. Shirai, and N. Layadi, J. Non-Cryst. Solids, 164-166, 989 (1993).

[54] K. Nomoto, Y. Urano, J. L. Guizot, G. Ganguly, and A. Matsuda, Jpn. J. Appl. Phys. 29, L1372 (1990).

[55] N. Shibata, K. Fukada, H. Ohtoshi, J. Hanna, S. Oda, and I. Shimizu, Mater. Res. Soc. Symp. Proc. 95, 225 (1987).

[56] Y. H. Yang, M. Katiyar, G. F. Feng, N. Maley, And J. R. Abelson, Appl. Phys. Lett. 65, 1769 (1994).

[57] S. Perkowitz, Optical Characterization of Semiconductors, Academic Press, New York, 1993.

[58] S. Lee, S. Kumar, and C. Wronski, A Critical Investigation of a-Si: H Photo Conductivity Generated by Sub-gap Absorption of light, J. Non-Cryst. Solids, 114, 316 (1989).

[59] J. Kocka, A. Fejfar, H. Stuchlikova, J. Stuchlik, P. Fojtk, T. Mates, B. Rezek, K. Luterova, V. Svcerk, and I. Pelant, Basic Features of transport in microcrystalline silicon, Solar Ennergy Materials & Solar Cells, 2002.

[60] A. M. Goodman, J. Appl. Phys. 32 (1961) 2520.

[61] Yong Liu, High growth rate deposition of hygrogenated amorphous silicon-germanium films and devices using ECR_PECVD, Ph.D. thesis, Iowa State University, 2002.

[62] J. Madhusudan, D. Debajyoti, and A.K. Barua, Role of hydrogen in controlling th egrowth of μ c-Si:H films from argon diluted siH4 plasma, Journal of Applied Physics, 2002 American Institute of Physics.

[63] A. Matsuda, J. Non-Cryst. Solids, 59 & 60, 767 (1983).

[64] S. Veprek, Mater. Res. Soc. Symp. Proc., 164, 39 (1990).

[65] N. Nanamura, K. Yoshida, S. Takeoka, and I. Shimizu, Jpn. J. Appl. Phys., Part 1 34, 442 (1995).

ACKNOWLEDGEMENTS

I would like to express my sincerely appreciation to Dr. Vikram Dalal for his invaluable guidance and continuing support throughout the course of this research project. I would also like to thank Dr. Robert J. Weber, Dr. Joseph Shinar, Dr. Gary Tuttle and Dr. Alan Constant for serving on my committee.

My thanks also go to Ms. Kay Han, Mr. Max Noack and Matt Welsh for their help with sample preparation and instrument trouble shooting. I would also thankYong Liu, Andy Niu, Puneet Sharma, Durga Panda and Nanlin Wang for their useful discussions and help with sample characterizaion, Matt Ring and Josh Graves for helping cleaning substrates. Special thanks are to Ms. Jane Woline at MRC for her countless help during the past three and a half years. The years at MRC will always be great memories in my whole life.

Finally, I would take the chance to thank my wife, Li, for her support and love throughout the years.